AUTOIMMUNITY

MicroRNA-142-3p shuttling in extracellular vesicles marks regulatory T cell dysfunction in multiple sclerosis

Giusy De Rosa[1,2], Claudia Russo[1,3], Silvia Garavelli[1], Dario Di Silvestre[4], Ilaria Spatocco[2], Giorgia Mele[2], Claudia La Rocca[1], Alessandra Colamatteo[2], Fortunata Carbone[1,5], Clorinda Fusco[1,3], Fabiana Passaro[2], Donatella Carpi[6], Elena Tagliabue[7], Francesco Prattichizzo[7], Francesca Brambilla[4], Pierluigi Mauri[1,4], Mirjam Hoxha[8], Valentina Bollati[8], Ilaria Giusti[9], Vincenza Dolo[9], Paola D'Antona[10], Paola Campomenosi[10], Valentina Mangolini[11,12], Annalisa Radeghieri[11,13], Paolo Bergese[11,13,14], Ivana Morabito[15], Alessandra Mandelli[15], Annamaria Finardi[15], Francesca Beretta[16], Edoardo Dalmato Schilke[17,18], Guido Cavaletti[16,17], Ettore Dolcetti[19], Fabio Buttari[19,20], Gianmarco Abbadessa[21,22], Simona Bonavita[21], Giacomo Lus[21], Elisabetta Signoriello[23], Roberta Lanzillo[24,25], Vincenzo Brescia Morra[24,25], Maria Mottola[26], Bruno Zuccarelli[26], Antonio Uccelli[27,28], Marco Salvetti[19,29], Diego Centonze[19,20], Roberto Furlan[15,30], Giuseppe Matarese[1,2,3], Claudio Procaccini[1,5]*†, Paola de Candia[2]*†

$CD4^+CD25^{hi}FoxP3^+$ regulatory T cells (T_{reg} cells) are key controllers of immune self-tolerance, and their suppressive function is impaired in people with relapsing-remitting multiple sclerosis (pwRR-MS). Because the mechanisms underlying this condition are still ill-defined, we investigated the role of T_{reg} cell–derived extracellular vesicles (T_{reg}-EVs) in T_{reg} cell dysfunction observed in pwRR-MS. We found that T_{reg}-EVs from healthy individuals inhibit $CD4^+$ conventional T (T_{conv}) cells by shuttling miR-142-3p from the T_{reg} cell to the T_{conv} cell. There, miR-142-3p down-regulated mRNAs necessary for T_{conv} cell growth and effector functions, such as the redox controller cystine carrier SLC7A11. However, T_{reg} cells from pwRR-MS released EVs containing reduced amounts of miR-142-3p, resulting in impaired suppressive function. Furthermore, T_{reg}-EV miR-142-3p inversely correlated with the disability score and gadolinium-enhancing lesions in pwRR-MS. Together, our results elucidate a molecular mechanism involving miR-142-3p shuttled by T_{reg}-EVs in the control of immune self-tolerance and unveil its pathogenetic implications in human autoimmunity.

INTRODUCTION

Starting from the last years of the 20th century, the interest in cell-derived lipid bilayer–enclosed particles, collectively named extracellular vesicles (EVs), has exponentially grown (*1*). EVs are found across the three domains of life—Archaea, Bacteria, and Eukarya—and their biogenesis and release are involved in pivotal cellular processes, such as damage-associated molecular patterns, the senescence-associated secretory phenotype, and viral egress (*2*–*4*). Originally thought to mostly serve as a waste disposal system for the extrusion of obsolete cellular molecules, EVs are instead at the center of multifaceted communication mechanisms based on the functional cell-to-cell transfer of their molecular cargo (*1*). In particular, an impressive amount of experimental work has progressively unveiled the participation of EVs in fundamental immunological processes, such as allergic, antimicrobial, and antitumor responses (*5*). As a relevant example, EVs contribute to the communication between T lymphocytes and antigen-presenting cells

[1]Laboratorio di Immunologia, Istituto degli Endotipi in Oncologia, Metabolismo e Immunologia "G. Salvatore", Consiglio Nazionale delle Ricerche (IEOMI-CNR), 80131 Napoli, Italy. [2]Dipartimento di Medicina Molecolare e Biotecnologie Mediche, Università degli Studi di Napoli Federico II, 80131 Napoli, Italy. [3]Azienda Ospedaliera Universitaria Federico II, 80131 Napoli, Italy. [4]Istituto di Tecnologie Biomediche, Consiglio Nazionale delle Ricerche (ITB-CNR), 20054 Segrate (MI), Italy. [5]Unità di Neuroimmunologia, IRCCS Fondazione Santa Lucia, 00179 Roma, Italy. [6]Joint Research Centre, 21027 Ispra (Varese), Italy. [7]IRCCS MultiMedica, 20138 Milano, Italy. [8]Laboratorio di Epidemiologia Molecolare e Epigenetica Ambientale, Dipartimento di Scienze Cliniche e di Comunità, Università degli Studi di Milano, 201122 Milano, Italy. [9]Dipartimento di Medicina Clinica, Sanità Pubblica, Scienze della Vita e dell'Ambiente, Università de L'Aquila, 67100 L'Aquila, Italy. [10]Dipartimento di Biotecnologie e Scienze della Vita, Universita' degli Studi dell'Insubria, 21100 Varese, Italy. [11]Dipartmento di Medicina Molecolare e Traslazionale, Università degli Studi di Brescia, 25123 Brescia, Italy. [12]IRCCS Fondazione Don Carlo Gnocchi ONLUS, 20148 Milano, Italy. [13]Consorzio Sistemi a Grande Interfase (CSGI), Dipartmento di Chimica, Università degli Studi di Firenze, 50019 Firenze, Italy. [14]IRIB - Institute for Research and Biomedical Innovation of CNR, 90146 Palermo, Italy. [15]Clinical Neuroimmunology Unit, Institute of Experimental Neurology, Division of Neuroscience, IRCCS Ospedale San Raffaele, 20132 Milano, Italy. [16]Clinica Neurologica, Fondazione IRCCS San Gerardo dei Tintori, 20900 Monza, Italy. [17]Experimental Neurology Unit, Dipartimento di Medicina e Chirurgia, Università degli Studi di Milano-Bicocca, 20900 Monza, Italy. [18]Dottorato in Neuroscienze, Università degli Studi di Milano-Bicocca, 20900 Monza, Italy. [19]Unità di Neurologia, IRCCS Neuromed, 86077 Pozzilli (IS), Italy. [20]Dipartmento di Medicina dei Sistemi, Università degli Studi di Roma Tor Vergata, 00133 Roma, Italy. [21]Dipartimento di Scienze Mediche e Chirurgiche Avanzate, Università degli Studi della Campania Luigi Vanvitelli, 80131 Napoli, Italy. [22]Department of Brain Sciences, Imperial College London, London SW7 2BX, UK. [23]Seconda Divisione di Neurologia, Azienda Ospedaliera Universitaria Luigi Vanvitelli, 80131 Napoli, Italy. [24]Dipartimento di Neuroscienze e Scienze Riproduttive ed Odontostomatologiche, Università degli Studi di Napoli Federico II, 80131 Napoli, Italy. [25]Unità di Sclerosi Multipla, Ospedale Policlinico, Università degli Studi di Napoli Federico II, 80131 Napoli, Italy. [26]Unità Operativa Complessa di Medicina Trasfusionale, Azienda Ospedaliera Specialistica dei Colli, 80131 Napoli, Italy. [27]IRCCS Ospedale Policlinico San Martino, 16132 Genova, Italy. [28]Dipartimento di Neuroscienze, Riabilitazione, Oftalmologia, Genetica e Scienze Materno-infantili, Università degli Studi di Genova, 16132 Genova, Italy. [29]Centro di Neurologia e Terapie Sperimentali, Dipartimento di Neuroscienze, Salute Mentale ed Organi di Senso, Università di Roma Sapienza, 00189 Roma, Italy. [30]Università Vita-Salute San Raffaele, 20132 Milano, Italy.
†These authors contributed equally to this work.
*Corresponding author. Email: paola.decandia@unina.it (P.d.C); claudio.procaccini@cnr.it (C.P.)

occurring at the immune synapse, a process at the very base of adaptive cellular immunity and antibody production, by shuttling key transcellular signals, such as proteins and microRNAs (miRNAs) (*6*–*10*).

In the past decade, EVs have also been evaluated for a more comprehensive understanding of the biology of $CD4^+CD25^+FoxP3^+$ regulatory T cells (T_{reg} cells), which safeguard immunological self-tolerance and inhibit aberrant or exaggerated immune responses by curbing the action of proinflammatory immune cells, including $CD4^+CD25^-FoxP3^-$ conventional T (T_{conv}) cells (*11*, *12*). In addition to the traditionally recognized mechanisms of T_{reg} cell action, more recent results indicate that murine T_{reg} cells may also suppress dendritic and effector T cells by releasing EVs, which function through both protein-dependent mechanisms and miRNA-mediated non–cell-autonomous gene silencing (*13*–*16*). Although the study of human T_{reg} cells is hampered by their difficult purification and numerical exiguity, prior work has shown that EVs released by those cells (T_{reg}-EVs) shuttle a different fingerprint of miRNA cargo compared with those released by the other T cell subsets and that T_{reg}-EVs hamper T cell–mediated proinflammatory activity (*17*–*19*). However, the mechanisms involved in the suppressive function of human T_{reg}-EVs are largely unexplored. Moreover, whether the T_{reg} cell functional impairment reported in autoimmune conditions such as multiple sclerosis (*20*–*23*) may also be, at least in part, due to defective EV release is still unknown. By thoroughly analyzing human $CD4^+$ T cells upon exposure to T_{reg}-EVs in terms of gene expression, signaling pathways, proliferative potential, and effector function, we have discovered that T_{reg}-EV biological function may represent a pathogenetic node contributing to the breach of immune self-tolerance in individuals with multiple sclerosis.

RESULTS

Human T_{reg}-EVs hamper the activation, proliferation, and effector phenotype of $CD4^+$ T cells

The nanometric EVs released by human $CD4^+$ T helper cell (T_H cell) subsets upon T cell receptor (TCR) stimulation in vitro and isolated through size exclusion chromatography (SEC) have been previously characterized (*17*, *24*) and have now been further analyzed for several features (https://evtrack.org/, #EV210300), including size and morphology (fig. S1, A and B). To dissect the biological function of T_{reg}-EVs in humans, we set up an in vitro system in which TCR-stimulated $CD4^+$ T cells were treated with allogeneic T_{reg}-EVs or the EVs released by the correspondent T_{conv} cells (T_{conv}-EVs) isolated from the same donor (in a 1:1 ratio of EV-releasing:EV-recipient cells) or with a mock EV preparation from unconditioned medium (controls) (Fig. 1A). Compared with $CD4^+$ T cells treated with T_{conv}-EVs, those exposed to T_{reg}-EVs formed fewer clusters upon TCR stimulation, appeared smaller in size, and showed higher viability, although no difference was observed in apoptotic cell death (Fig. 1, B to E). T_{reg}-EVs also reduced the expression of three key activation markers—CD25, CD69, and OX-40—on $CD4^+$ T cells; decreased the phosphorylation of the linker of activation of T cells (LAT), the extracellular signal-regulated kinase 1/2 (ERK1/2), and the mammalian target of rapamycin (mTOR) target S6; and enhanced the quantity of the cyclin-dependent kinase inhibitor $p27^{Kip1}$, thus revealing the interference of T_{reg}-EVs in TCR-mediated activation signals (Fig. 1, F to K).

Furthermore, T_{reg}-EVs, compared with controls and T_{conv}-EVs, reduced $CD4^+$ T cell proliferation, as assessed by impaired CellTrace violet dilution (Fig. 1, L and M) and a DNA incorporation tracking assay (fig. S1, C to E). T_{reg}-EVs also affected $CD4^+$ T_H cell polarization and function because they reduced the frequency of cells expressing T-box transcription factor (T-bet), GATA binding protein 3 (GATA3), and retinoic acid–related orphan receptor γt (RORγt) (master orchestrators of T_H1, T_H2, and T_H17 cell subset differentiation, respectively) while not affecting the frequency of cells expressing FoxP3 (master regulator of T_{reg} cells), when compared with cells exposed to either controls or T_{conv}-EVs (Fig. 1, N to Q); T_{reg}-EVs also inhibited the secretion of proinflammatory cytokines [e.g., interferon-γ (IFN-γ), tumor necrosis factor–α (TNF-α), and interleukin-17A (IL-17A)], relative to cells treated with either controls or T_{conv}-EVs (Fig. 1R and fig. S1F). At the protein level, T_{reg}-EVs specifically imprinted $CD4^+$ T cell targets, as demonstrated by proteomics clustering analysis (Fig. 1S); in particular, T_{reg}-EVs decreased IFN-dependent cell activity and macromolecular catabolism, including proteolysis, and enhanced the expression of the Runt-related transcription factor 3 (RUNX3) pathway, known to hamper T cell functional activation (Fig. 1, T and U; fig. S2; and data files S1 and S2).

The antiproliferative effect of T_{reg}-EVs on target $CD4^+$ T cells was comparable (same order of magnitude) to that of T_{reg} cells themselves (fig. S3A). Confirming the contribution of EVs to T_{reg} cell suppressive activity, we observed that T_{reg} cells treated with an inhibitor of EV release (GW4869) (*25*) delivered substantially lower amounts of miR-142-3p and miR-150-5p (two miRNAs known to be highly expressed in $CD4^+$ T cells) (*26*) as compared with vehicle-treated cells (fig. S3, B and C) and were significantly less proficient in suppressing $CD4^+$ T cell proliferation ($P < 0.0001$) and activation (%CD25, $P < 0.0001$; %CD69, $P < 0.0001$; and %OX40, $P < 0.01$) in coculture experiments as compared with vehicle-treated cells (fig. S3, D to H). Furthermore, the suppressive activity of T_{reg}-EVs did not depend on the specific EV purification method used (SEC) because small (but not large) T_{reg}-EVs isolated by differential centrifugation (100,000*g* versus 16,000*g*, respectively) were also able to reduce $CD4^+$ T cell growth, as compared with T_{conv}-EVs prepared with the same procedure (fig. S3, I to K).

After having verified that human T_{reg}-EVs were able to also hamper murine $CD4^+$ T cell proliferation and activation (fig. S3, L to R), we injected human T_{reg}-EVs into mice with experimental autoimmune encephalomyelitis [EAE; a mouse model of human multiple sclerosis, (*27*)] to test the capability of T_{reg}-EVs to lower inflammatory processes in vivo. In detail, EAE was induced in C57BL/6 mice by immunization with myelin oligodendrocyte glycoprotein (MOG_{35-55}) peptide, and, upon symptom appearance [12 days postimmunization (p.i.)], mice were randomized and intraperitoneally injected for 3 consecutive days (days 12 to 14 p.i.) with either T_{reg}-EVs or controls ($n = 20$ or 21 mice, respectively); then, they were euthanized 25 days p.i. (fig. S4A). Compared with control, T_{reg}-EV treatment was found to decrease maximum disease severity (fig. S4, B to F) and perivascular immune cell infiltration in the central nervous system (CNS), although no marked differences were observed in EAE cumulative score, demyelination area, and axonal loss (fig. S4, G to J). Specifically, the $CD8^+$ T cell component of the CNS-infiltrating leukocytes expressed significantly ($P < 0.05$) lower amounts of the migratory marker CC chemokine receptor type 5 (CCR5) in mice treated with T_{reg}-EVs, suggesting that the capacity of those key pathogenetic lymphocytes to reach the CNS may be partially impaired (fig. S4K). Regarding the myeloid component ($CD11b^+$ cells) within the CNS, mice treated with T_{reg}-EVs,

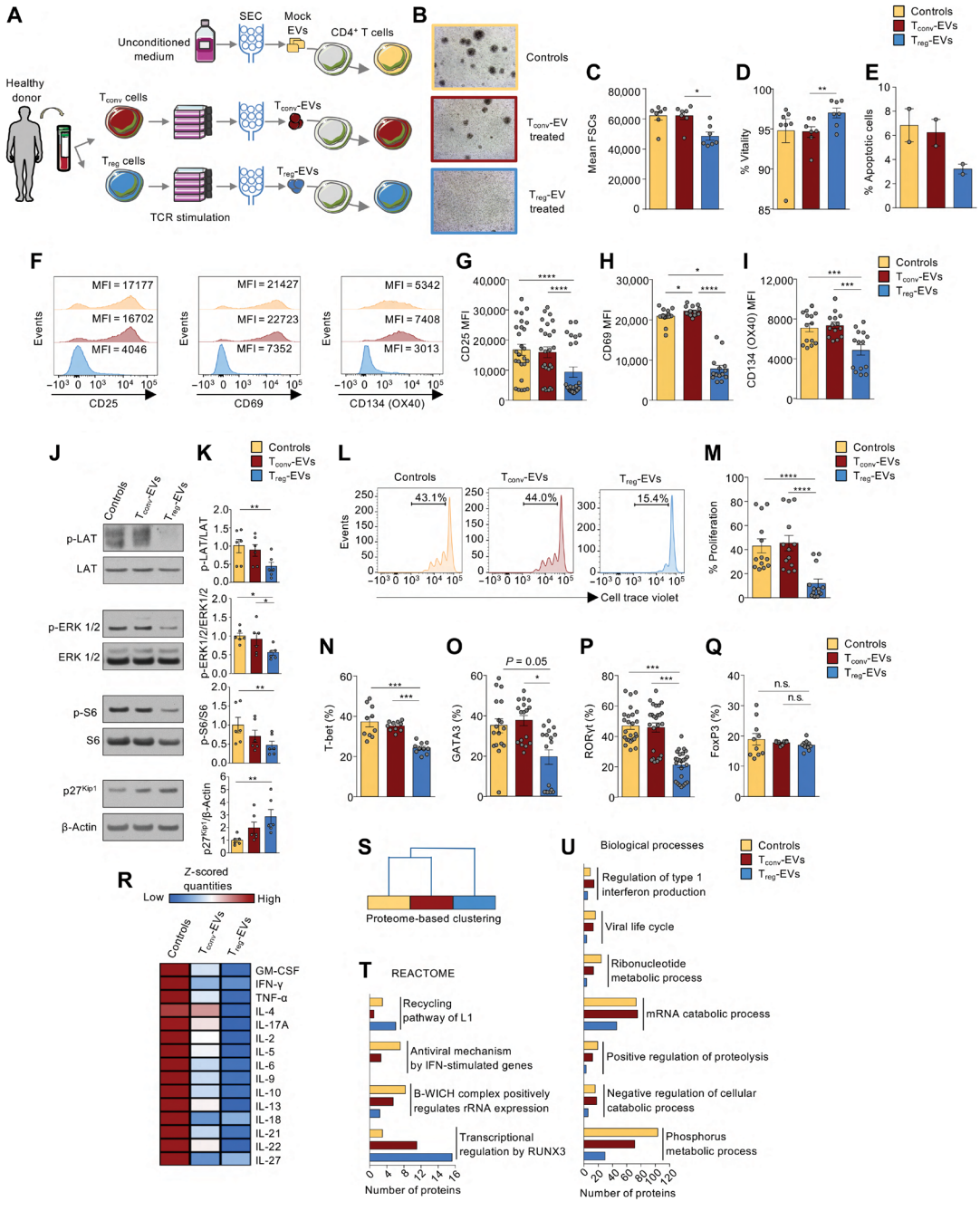

Fig. 1. Human T_{reg}-EVs hamper $CD4^+$ T cell growth and effector functions. (**A**) Schematic outline summarizing the experimental flow from $CD4^+$ T cell isolation and in vitro TCR stimulation to EV purification by SEC and EV treatment of allogenic in vitro TCR-stimulated $CD4^+$ T cells. (**B**) Representative optic microscope pictures of activation-dependent cellular clustering of TCR-stimulated $CD4^+$ T cells treated as indicated. (**C** to **E**) Bar graphs (means ± SEM with all experimental points) showing the cell size as forward-scatter (FSC) (C) and the percentage of vital cells (D) ($n = 7$ from four independent experiments) and caspase-dependent apoptotic cells [(E), from two independent experiments] as assessed by flow cytometry analysis of TCR-stimulated $CD4^+$ T cells treated as indicated. (**F** to **I**) Representative experiment (F) and bar graphs (means ± SEM with all experimental points) showing the mean fluorescence intensities (MFIs) of CD25 (G), CD69 (H), and CD134 (OX40) (I) as assessed by flow cytometry analysis of TCR-stimulated $CD4^+$ T cells treated as indicated (minimum $n = 14$ from six independent experiments). (**J** and **K**) Immunoblotting of the reported signaling proteins [one representative experiment, (J)] and relative normalized quantifications [mean fold change versus controls ± SEM with all experimental points; minimum $n = 6$ measurements from two independent experiments, (K)] in TCR-stimulated $CD4^+$ T cells treated as indicated. (**L** and **M**) CellTrace violet dilution assay assessed by flow cytometry [one representative experiment, (L)] and bar graph [means ± SEM with all experimental points; $n = 13$ from seven independent experiments, (M)] showing the percentage of $CD4^+$ T cell proliferation upon TCR stimulation and the indicated treatments. (**N** to **Q**) Bar graphs (means ± SEM with all experimental points) showing the frequency of cells expressing the master regulators of T cell polarization, T-bet (N), GATA3 (O), RORγt (P), and FoxP3 (Q) as assessed by flow cytometry analysis of TCR-stimulated $CD4^+$ T cells treated as indicated (minimum $n = 10$ from at least two independent experiments). (**R**) Heatmap reporting the mean values (see also fig. S1F) of cytokine quantification through Luminex assay of the media of TCR-stimulated $CD4^+$ T cells treated as indicated (minimum $n = 21$ from 14 independent experiments). (**S**) Clustering analysis based on proteomics samples (mean of three independent experiments) from TCR-stimulated $CD4^+$ T cells treated as indicated. (**T** and **U**) Bar graphs showing the number of proteins leading to Reactome (T) and biological process (U) enrichment in the lists of expressed proteins [false discovery rate (FDR) < 0.05], as assessed by proteomics analysis of TCR-stimulated $CD4^+$ T cells treated as indicated (linear discriminant analysis, $P < 0.05$). Data were analyzed by Friedman's test with Dunn's correction for multiple comparisons [(C) to (E), (G) to (I), and (K)]; ordinary one-way ANOVA with Šidák's correction for multiple comparisons (M); or Kruskal-Wallis test with Dunn's correction for multiple comparisons [(N) to (Q)]. *$P < 0.05$; **$P < 0.01$; ***$P < 0.001$; ****$P < 0.0001$; n.s., not significant. GM-CSF, granulocyte-macrophage colony-stimulating factor; rRNA, ribosomal RNA.

compared with controls, showed a significantly ($P < 0.01$) lower percentage of neutrophils ($Ly6G^+$), known to exert a proinflammatory action in EAE. Moreover, those mice exhibited a significantly ($P < 0.05$) higher frequency of anti-inflammatory monocytes (characterized by low Ly6C expression), thus revealing a less aggressive inflammatory phenotype also at the level of innate immunity (fig. S4, L to N). Although there were no differences in the expression of the main pathogenic cytokines (*Tnfa*, *Ifng*, and *Il1b*), we did observe a slight increase in $FoxP3^+$ T_{reg} cell frequencies in the spleens of mice, suggesting a less pronounced splenic proinflammatory milieu in the T_{reg}-EV–treated mice (fig. S4, O and P); consistently, the frequency of splenic $FoxP3^+$ T_{reg} cells negatively correlated with the disease score (fig. S4Q). Collectively, these results support the hypothesis that human T_{reg}-EVs are able to dampen $CD4^+$ T cell activation, proliferation, proinflammatory phenotype, and effector functions in vitro and may exert a protective effect in autoimmune conditions, as suggested by mouse data.

MiR-142-3p is enriched in human and mouse T_{reg}-EVs

We then decided to correlate the observed biological function of T_{reg}-EVs with their specific molecular cargo. With this aim, 51 miRNAs [of 752 profiled by real-time quantitative polymerase chain reaction (RT-qPCR)] were initially found detectable [threshold cycle (Ct) < 35 in a minimum of four of the five donors] in T_{reg}-EVs, 38 of which were also found in the corresponding T_{conv}-EVs (GSE209714 and GSE183713) (Fig. 2A). The relative quantities of those 38 miRNAs, normalized by sample-based Ct global mean (which efficiently eliminated intersample quantitative variability, Fig. 2B), were able to discriminate the cellular origin of the EVs, as shown by clustering analysis (Fig. 2C). In particular, miR-142-3p was significantly ($P < 0.05$) up-regulated in T_{reg}-EVs compared with T_{conv}-EVs and also turned out to be the most abundant miRNA in T_{reg}-EVs, representing 25% of the 10 highest miRNAs; in contrast, miR-142-3p only ranked seventh in terms of quantitative representation in T_{conv}-EVs (Fig. 2, D and E). The 10 top-ranked miRNAs in T_{reg}-EVs are highly conserved between mice and humans (identical sequences of the mature miRNA molecules, with the only exception of hsa-miR-1260a, exclusively found in *Homo sapiens*; table S1); moreover, murine T_{reg}-EVs were able to shuttle significantly ($P < 0.05$) higher quantities of *mmu*-miR-142-3p compared with T_{conv}-EVs, suggesting a mammalian conservation of this specific T_{reg}-EV cargo feature (Fig. 2, F and G).

The capability of T cell–derived EVs to transfer miR-142-3p into the EV-target cells was evaluated by directly transfecting them with a miR-142-3p mimic (or the nonhuman *Cel*-miR-39-3p, as control) and registering the miRNA uptake by EV recipient $CD4^+$ T cells through RT-qPCR quantification and flow cytometry analysis (fig. S5, A to E). By tracing the EV-associated whole RNA with a selective fluorescent RNA stain (SYTOGreen RNASelect), $CD4^+$ T cell–derived EVs were demonstrated to shuttle their RNA cargo into most of heterologous target T cells upon 48 hours of EV treatment (fig. S5, F to H).

T_{reg}-EVs reduce transcripts linked to T cell activation, IFN signaling, and proteasomal function in TCR-stimulated $CD4^+$ T cells

We then evaluated the effect of EVs on the whole coding transcriptome of $CD4^+$ T cells and unveiled a distinct transcriptional profile of cells treated with T_{reg}-EVs compared with T_{conv}-EVs or controls [Fig. 3, A and B; RNA sequencing (RNA-seq) data: GSE208570]. Specifically, compared with controls, T_{reg}-EVs were able to significantly (adjusted $P < 0.05$) modulate 487 transcripts (330 up-regulated and 157 down-regulated), which only marginally overlapped with the list of transcripts modulated by T_{conv}-EVs (21 and 11% for up- and down-regulated transcripts, respectively; Fig. 3, C and D, and data file S3). Whereas the transcripts up-regulated by T_{reg}-EVs were mostly linked to cell cycle regulation, the list of down-regulated ones was instead highly enriched for IFN-related transcripts, consistent with the proteome data (Fig. 3, E and F). Furthermore, the transcripts down-regulated by T_{reg}-EVs were also enriched for those related to the proteasome complex and its regulation (in line with experimental evidence of decreased T cell proliferation upon inhibition of proteasome activity) (*28*) and others linked with the cell cycle, signal transduction, and antigen presentation (fig. S6, A to C), delineating a broad impairment of T cell activation at the transcriptional level, in the presence of T_{reg}-EVs. Consistently, the transcriptome modulation induced by T_{reg}-EVs (but not T_{conv}-EVs) in $CD4^+$ T cells was negatively correlated with that previously described in the same cells upon TCR stimulation [GSE154401 (*23*); Fig. 3, G and H], with transcripts encoding key activation-induced factors, such as CD109, CD69, IL-2Rα, IL-5, IL-6, IL-31, and REL, among others (*23*), all decreased by T_{reg}-EV treatment (Fig. 3I).

The antiporter *SLC7A11*, repressed by T_{reg}-EVs in $CD4^+$ T cells, is a direct target of miR-142-3p

The category of transcripts decreased by T_{reg}-EV treatment was significantly ($P < 0.00001$) enriched among miR-142-3p targets (as per miRTarBase release 8.0, 142 of 324, 44%), supporting the hypothesis that the biological effect of T_{reg}-EVs may be mediated, at least in part, by the higher relative quantities of EV-shuttled miR-142-3p, compared with T_{conv}-EVs (Fig. 4A). A similar enrichment was also true for the second most-abundant miRNA in T_{reg}-EVs, miR-21-5p (50%), whereas the effect started fading with the third and the fourth, miR-150-5p and miR-16-5p (33% of decreased transcripts in both cases), and disappeared with the fifth (miR-1260a, 28%); as a negative control, no enrichment was revealed for the targets of an unrelated miRNA (miR-1-3p, 31%, Fig. 4A). In particular, miR-142-3p mRNA targets down-regulated by T_{reg}-EVs were found to be specifically enriched for biological processes mostly linked to protein metabolism (including proteasomal genes, such as *PSMD11*, *PSMD12*, and *PSME4*) and fatty–acyl–coenzyme A metabolism (Fig. 4B and data file S4). Gene set enrichment analysis (GSEA) demonstrated that miR-142-3p targets were more densely clustered in the region of transcripts decreased by T_{reg}-EVs in comparison with either controls or T_{conv}-EVs, confirming that the targetome of this miRNA is marking T_{reg}-EV transcriptional effects (Fig. 4C).

Among the top 20 most–down-regulated transcripts by T_{reg}-EVs, we identified the transmembrane antiporter mediating cystine uptake and glutamate export *SLC7A11* as the most-repressed putative miR-142-3p target ($\log_2$ fold change = −1.03, data file S3). Furthermore, the enrichment score (ES), reflecting the degree to which miR-142-3p targets are overrepresented in the ranked gene list (transcriptional modulation by T_{reg}-EVs), identified *SLC7A11* as the top transcript among those driving the GSEA results (leading edge subset, Fig. 4D). Because the actual capability of miR-142-3p to directly target *SLC7A11* expression was only supported by weak experimental evidence (data file S4), we tested two plasmids in which the luciferase gene, under the control of a constitutive promoter, was cloned to bear the two putative miR-142-3p binding sequences of the *SLC7A11* mRNA in the 3′ untranslated region (3′UTR) (nucleotides at positions

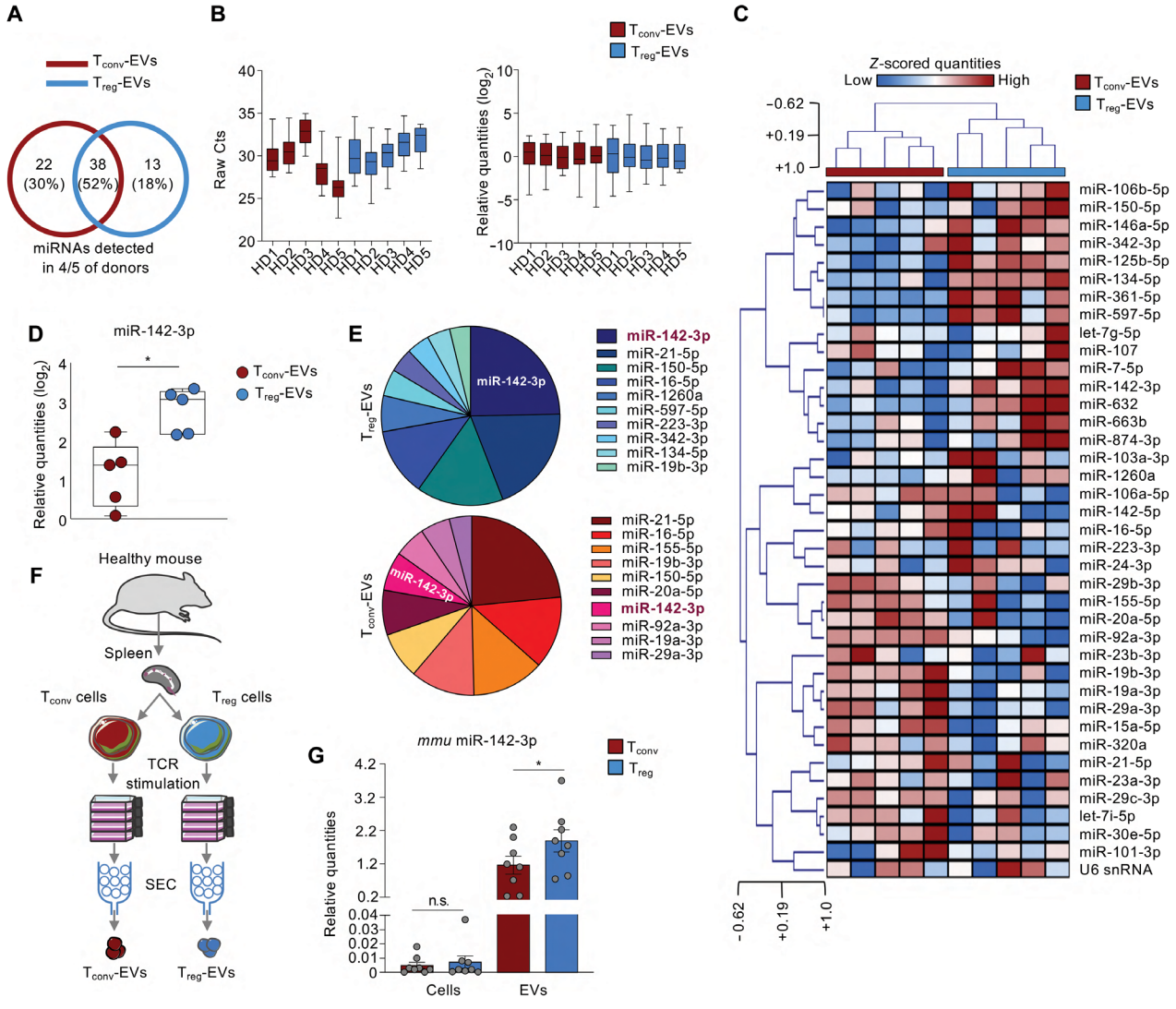

Fig. 2. High quantities of miR-142-3p molecular cargo characterize T_{reg}-EVs from healthy humans and mice. (**A**) Venn diagram showing the overlap ($n = 38$) of miRNAs detected (Ct < 35 by RT-qPCR profiling, $n = 179$ miRNAs) in at least four of the five independent donors of purified EVs released by both T_{conv} and T_{reg} cells. (**B**) Box and whisker plots [min to max with median and interquartile range (IQR)] showing the Ct values (left) and the quantities relative to the Ct global mean (right) of the 17 miRNAs coexpressed in five of the five samples of T_{conv}-EVs and T_{reg}-EVs, showing an efficient normalization procedure. (**C**) Heatmap showing the hierarchical clustering (based on Pearson correlation with complete linkage) of T_{conv}-EV and T_{reg}-EV samples on the basis of the expression of EV-associated miRNA profiles [$n = 38$ coexpressed molecules, as for (A)]. (**D**) Box and whisker plot (min to max with median and IQR, including all five experimental points) reporting the quantities (relative to Ct global mean) of miR-142-3p in T_{conv}-EV and T_{reg}-EV samples. (**E**) Pie charts showing the mean quantitative representation of the first 10 most-expressed miRNAs in T_{reg}-EVs (top) and T_{conv}-EVs (bottom); the ranking position of miR-142-3p in the two EV subtypes is highlighted. (**F** and **G**) Schematic outline summarizing the experimental flow for mouse $CD4^+$ T cell and T cell–derived EV purification (F) and bar graph (means ± SEM with all experimental points) reporting the quantities (as assessed by RT-qPCR, $n = 8$ from four independent biological replicates) of miR-142-3p in $CD4^+$ T cells and T cell–derived EVs, as indicated (G). Data were analyzed by Mann-Whitney test (D) or Wilcoxon matched-pairs rank test (G). *$P < 0.05$; n.s., not significant.

3301 to 3308 and 5397 to 5403, TargetScanHuman 7.0; Fig. 4E). The luciferase assay in human embryonic kidney (HEK)–293 cells transfected with those plasmids allowed us to demonstrate that only one of the two tested seeding sites (5397 to 5403, highly conserved in mammalian genomes; table S2) specifically responds to miR-142-3p–dependent regulation (Fig. 4F). Consistently, $CD4^+$ T cell–derived EVs transfected with a miR-142-3p mimic, compared with mock-transfected ones, significantly decreased SLC7A11 at the protein level in Jurkat cells ($P < 0.01$) and in primary human $CD4^+$ T cells ($P < 0.0001$) (Fig. 4, G to J). The hypothesis that miR-142-3p shuttled by T_{reg}-EVs is able to target *SLC7A11* (and other relevant mRNAs) in bystander $CD4^+$ T cells may have important mechanistic implications, which pertain to both T_{reg} cell suppressive function and the potential therapeutic use of T_{reg}-EVs. We thus decided to further investigate the dynamics of

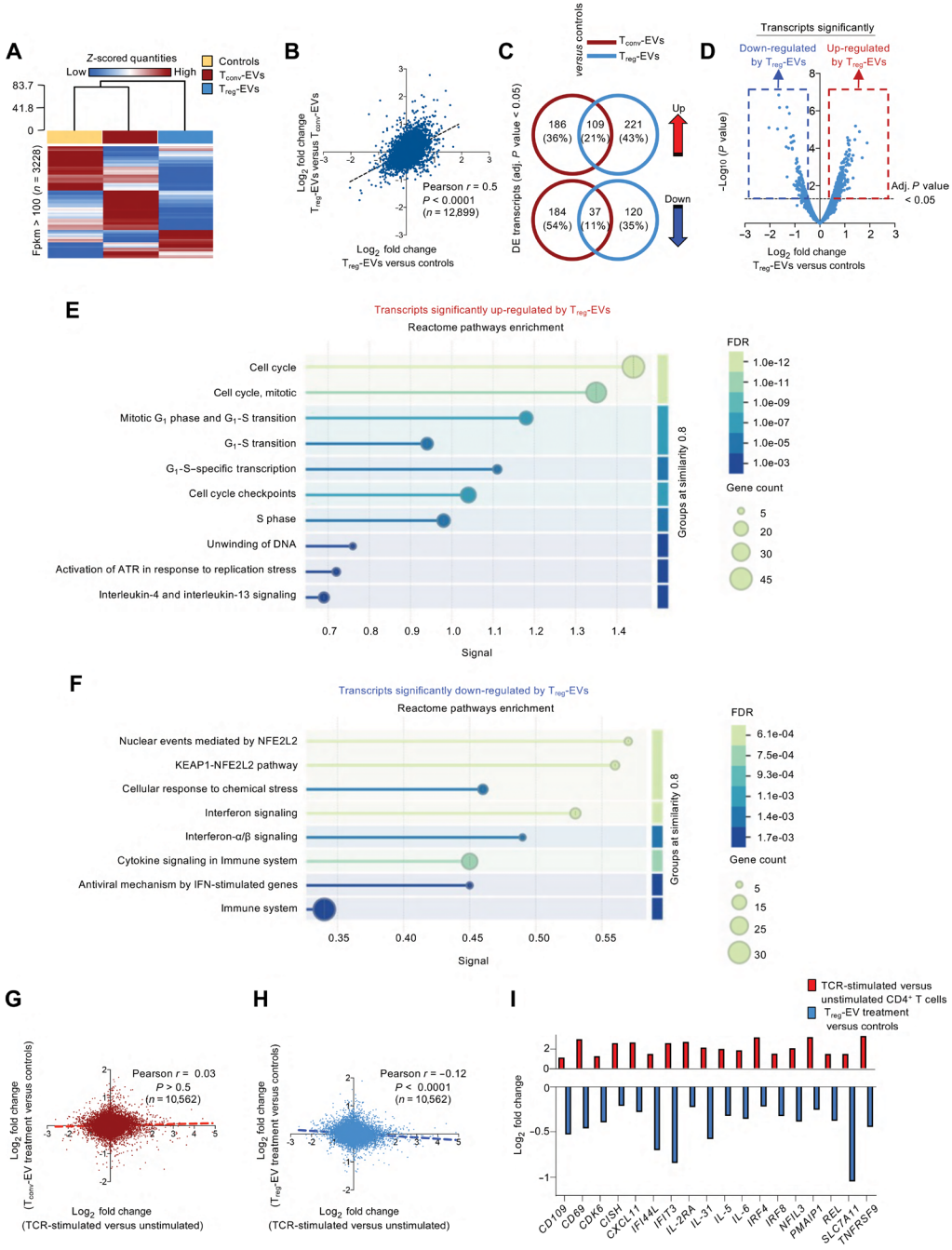

Fig. 3. Transcriptomics of CD4$^+$ T cells treated with human T_{reg}-EVs. (**A**) Heatmap showing the hierarchical clustering (as determined by Euclidean distance with complete linkage) of RNA-seq samples (mean of three independent biological samples) from TCR-stimulated CD4$^+$ T cells treated as indicated. (**B**) Scatter plot showing the correlation between the $\log_2$ fold changes in the comparisons T_{reg}-EVs versus controls, *x* axis, and T_{reg}-EVs versus T_{conv}-EVs, y axis, for the RNA-seq of TCR-stimulated CD4$^+$ T cells. Pearson correlation coefficient (*r*), *P* value, and transcript numbers are also reported. (**C**) Venn diagrams reporting the overlap in terms of differentially expressed (DE) transcripts (adjusted $P < 0.05$) for the indicated RNA-seq comparisons, stratified for being either up-regulated (top) or down-regulated (bottom) versus controls. (**D**) Volcano plot reporting the fold changes (*x* axis) and $-\log_{10}$ *P* values (*y* axis) for RNA-seq expression in TCR-stimulated CD4$^+$ T cells treated with T_{reg}-EVs versus controls. (**E** and **F**) STRING analysis showing the Reactome pathway enrichments for the list of transcripts significantly (adjusted $P < 0.05$) either up-regulated (E) or down-regulated (F) by T_{reg}-EVs. (**G** and **H**) Scatter plots showing the correlations between the RNA-seq fold changes [T_{conv}-EV (G) and T_{reg}-EV (H), treatments versus controls] and the transcriptional modulation reported in CD4$^+$ T cells upon TCR stimulation. (**I**) Bar graph showing the RNA-seq fold changes of biologically relevant transcripts down-regulated upon T_{reg}-EV treatment versus controls (blue) previously reported to be up-regulated (red) in CD4$^+$ T cells upon TCR stimulation, independently of statistical significance. Fpkm, fragments per kilobase million; *ATR*, *ataxia telangiectasia and Rad3 related*; *CDK6*, *cyclin-dependent kinase 6*; *CISH*, *cytokine-inducible SH2-containing protein*; *CXCL11*, *C-X-C motif chemokine ligand 11*; *IFI44L*, *interferon-induced protein 44-like*; *IFIT3*, *interferon induced protein with tetratricopeptide repeats 3*; *IL2RA*, *interleukin 2 receptor subunit alpha*; *IRF4*, *interferon regulatory factor 4*; *IRF8*, *interferon regulatory factor 8*; *KEAP1*, *Kelch-like ECH-associated protein 1*; *NFE2L2*, *nuclear factor erythroid-derived 2-like 2*; *NFIL3*, *nuclear factor interleukin-3*; *PMAIP1*, *phorbol-12-myristate-13-acetate-induced protein 1*; *SCL7A11*, *solute carrier family 7 member 11*; *TNFRSF9*, *TNF receptor superfamily member 9*.

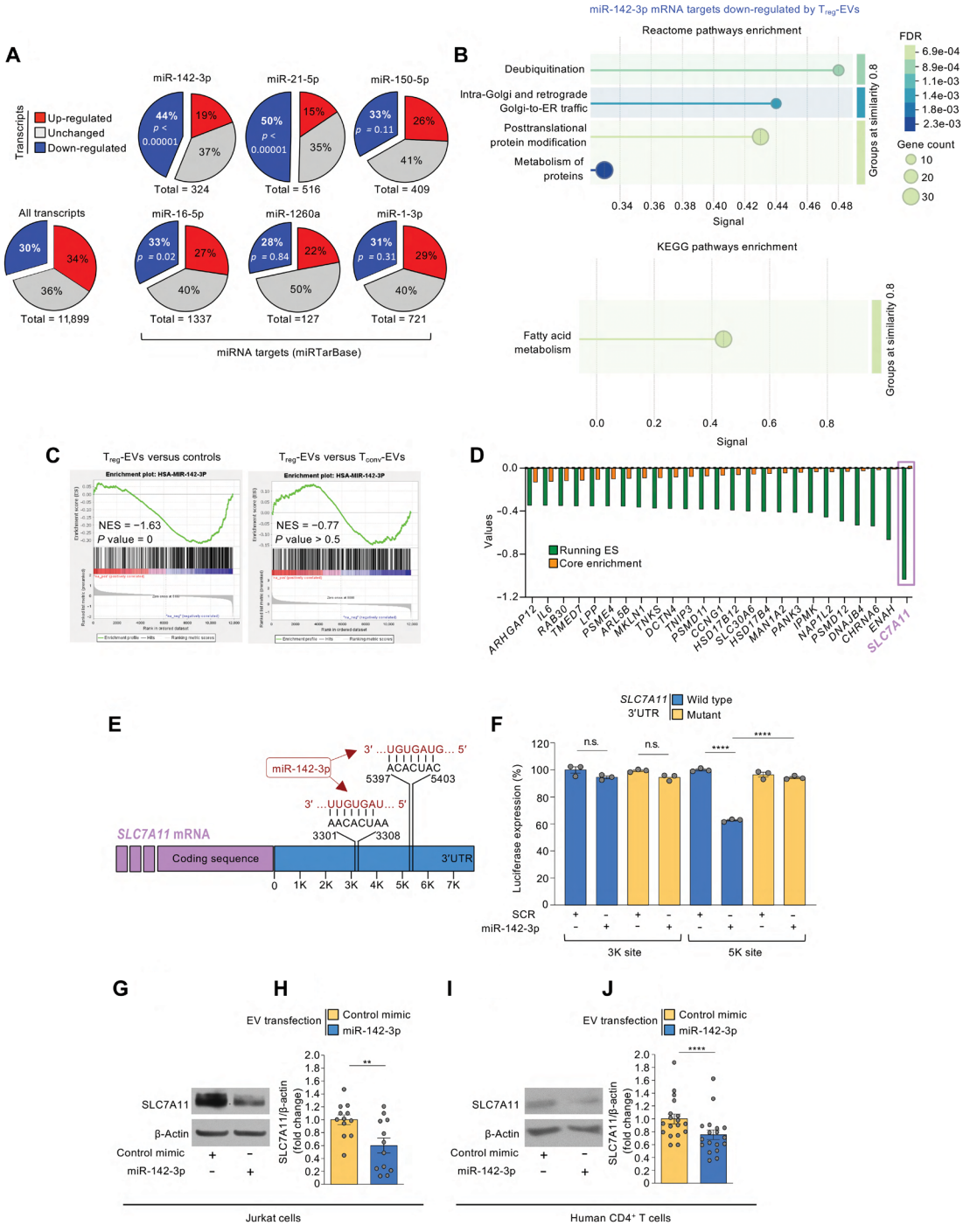

Fig. 4. CD4$^+$ T cell transcripts down-modulated by human T_{reg}-EVs are enriched for miR-142-3p mRNA targets. (**A**) Pie charts showing the distribution of transcripts that are up-regulated (red, $\log_2$ fold change > 0.1), unchanged (gray, −0.1 < $\log_2$ fold change < 0.1), or down-regulated (blue, $\log_2$ fold change < −0.1) in the RNA-seq comparison of TCR-stimulated CD4$^+$ T cells treated with T_{reg}-EVs versus controls; either all detected transcripts (n = 11,899) or the list of the targets (as per miRTarBase) of the indicated miRNAs are plotted; miR-1 was used as a negative control, not being expressed in T_{reg}-EVs. Fisher's exact test. (**B**) STRING analysis showing the Reactome and Kyoto Encyclopedia of Genes and Genomes (KEGG) pathway enrichments on the basis of the list of miR-142-3p–validated mRNA targets (as per miRTarBase) down-regulated by T_{reg}-EVs versus controls. (**C**) GSEA based on the list of miR-142-3p validated mRNA targets for the transcriptional fold change reported in the RNA-seq comparison of T_{reg}-EVs versus controls (left) or T_{reg}-EVs versus T_{conv}-EVs (right); normalized enrichment scores (NESs) and P values are also reported. (**D**) Column bar plot showing the running ES (green) and the core enrichment (orange) for the top-ranked gene list driving the GSEA enrichment for miR-142-3p targets. *SLC7A11* is highlighted. (**E**) Schematic representation of the *SLC7A11* transcript, reporting the positions of two putative seed sites for miR-142-3p present in the 3′UTR region of the transcript. (**F**) Bar graph (means ± SEM with all experimental points) reporting the luciferase assay performed in HEK-293 cells (n = 3 independent experiments), testing the ability of a miR-142-3p mimic molecule to functionally bind the identified seed sites in the *SLC7A11* 3′UTR. (**G** to **J**) Immunoblotting [representative experiments, (G) and (I)] and the corresponding quantifications [bar graphs reporting the means ± SEM with all experimental points, (H) and (J)], comparing the relative capacity of CD4$^+$ T cell–derived EVs (derived from HDs) transfected with a miR-142-3p mimic molecule or with a control mimic to decrease the quantity of SLC7A11 protein in both EV-treated Jurkat cells (n = 12 measurements from four independent experiments) [(G) and (H)] and allogeneic human CD4$^+$ T cells (n = 18 from five independent experiments) [(I) and (J)]. Control mimic was set to 1. Data were analyzed by ordinary one-way ANOVA with Holm-Šídák's correction for multiple comparisons (F) or paired t test [(H) and (J)]. **P < 0.01; ****P < 0.0001; n.s., not significant.

miR-142-3p and *SLC7A11* transcript modulation in CD4$^+$ T cells upon TCR stimulation and T_{reg}-EV treatment.

MiR-142-3p shuttled by T_{reg}-EVs impinges on the highly tuned regulation of the *SLC7A11* antiporter upon TCR stimulation

SLC7A11 mRNA induction during activation of CD4$^+$ T cells is a key determinant of their proliferative potential (*23*, *29*). Upon TCR stimulation, *SLC7A11* expression in CD4$^+$ T cells was predominant (>65%) in CD25$^+$ T cells (the activated subpopulation), whereas it remained marginal (<5%) in CD25$^-$ cells (Fig. 5A). T_{reg}-EV–mediated inhibition of CD25 expression was accompanied by a significant reduction in the percentage of *SLC7A11*-expressing cells ($P < 0.01$) and their mean fluorescence intensity ($P < 0.05$) (Fig. 5, B to D). The measurement of RNA molecules at single-cell resolution by PrimeFlow assay (Fig. 5E) allowed for contextualizing the dynamics of miR-142-3p and *SLC7A11* transcript quantities together with CD25 protein expression by flow cytometry. CD4$^+$ T cell activation modified the quantitative relation between *SLC7A11* and miR-142-3p, with the miRNA quantities growing less than those of the mRNA in the CD25$^+$ compared with the CD25$^-$ T cell subpopulation, thus leading to a reduced miR-142-3p/*SLC7A11* ratio in the activated (CD25$^+$) cells independently of EV treatment (Fig. 5, F and G, and fig. S6D). Nonetheless, T_{reg}-EVs were specifically shown to unbalance the regulatory circuit between miR-142-3p and *SLC7A11* mRNA during T cell activation by significantly increasing the miR-142-3p/*SLC7A11* ratio in both CD25$^-$ ($P < 0.05$) and CD25$^+$ ($P < 0.001$) T cell subpopulations compared with controls (Fig. 5H). These observations suggested that the uptake of T_{reg}-EV cargo in CD4$^+$ T cells raises the intracellular amounts of miR-142-3p relative to its targets (mRNAs necessary to engage growth and effector functions, such as *SLC7A11*), thus hampering the induction of those proteins during the process of cellular activation.

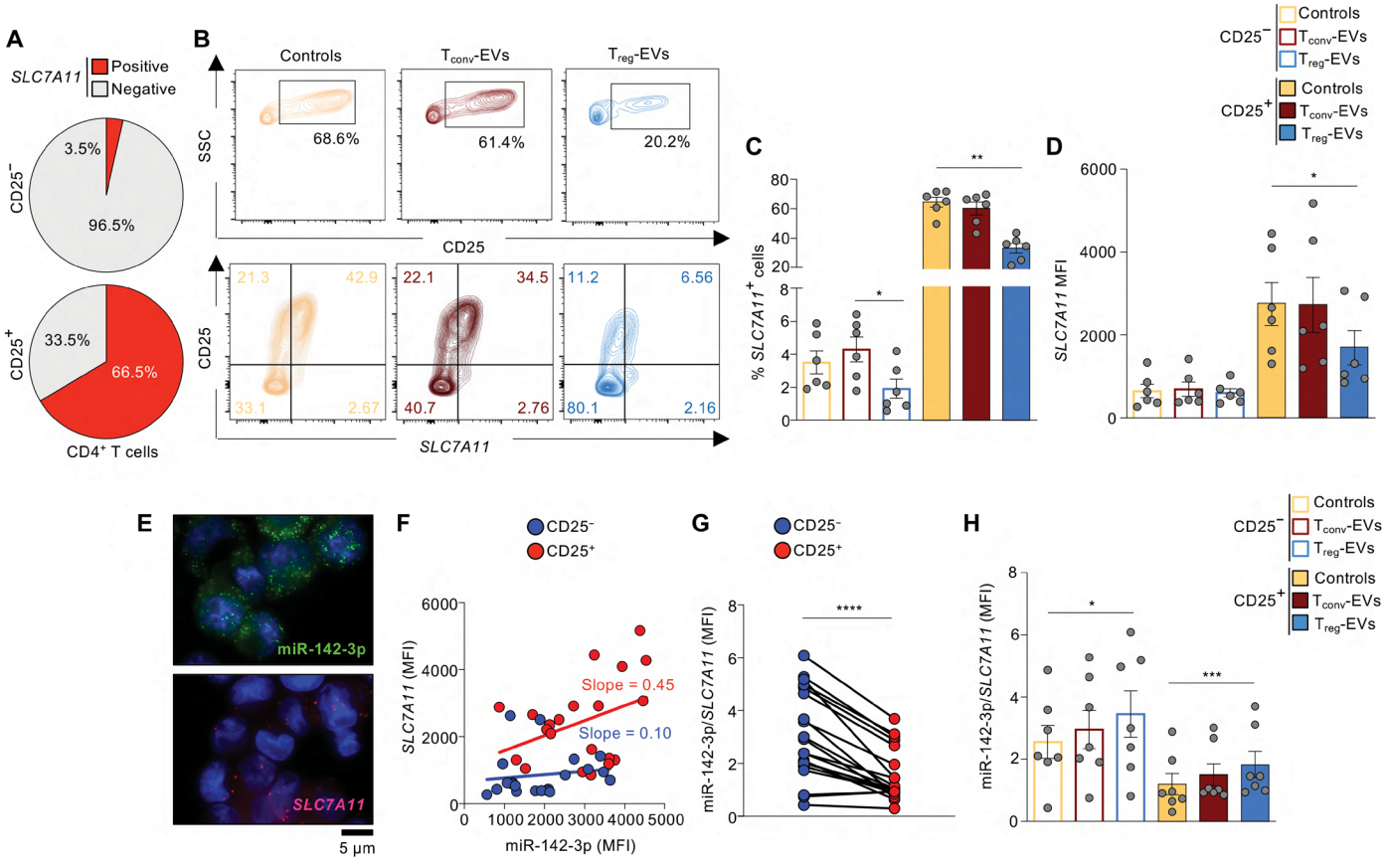

Fig. 5. Human T_{reg}-EVs regulate miR-142-3p/*SLC7A11* ratio tuning occurring upon CD4$^+$ T cell stimulation. (**A**) Pie charts showing the relative percentage of cells expressing *SLC7A11* mRNA in either CD25$^+$ (red) or CD25$^-$ (gray) CD4$^+$ T cells upon TCR stimulation in the absence of any EV treatment. (**B** to **D**) Contour plots [one representative experiment, (B)] and bar graphs (means ± SEM with all experimental points) showing the percentage (C) and the MFI (D) of *SLC7A11* mRNA in either CD25$^-$ (empty bars) or CD25$^+$ (filled bars) TCR-stimulated CD4$^+$ T cells upon the indicated EV treatments ($n = 6$ from six independent experiments). SSC, side scatter. (**E**) Two representative microscope images of the intracellular PrimeFlow fluorescent signal of miR-142-3p (green, top) and *SLC7A11* mRNA (red, bottom) (scale bar, 5 µm). (**F**) Scatter plot showing the linear correlation between the miR-142-3p MFI (*x* axis) and that of *SLC7A11* mRNA (*y* axis) in either CD25$^+$ (red, $r = 0.37$) or CD25$^-$ (blue, $r = 0.27$) CD4$^+$ T cells upon TCR stimulation independently of EV treatment; the two differential correlation slopes are also reported (based on 21 observations from six independent experiments). (**G**) Direct comparison (per single cell sample) of the miR-142-3p/*SLC7A11* ratio (expressed as MFI) in CD25$^+$ (red) versus CD25$^-$ (blue) CD4$^+$ T cells upon TCR stimulation independently of EV treatment (based on 21 observations from six independent experiments). (**H**) Bar graphs (means ± SEM with all experimental points) showing the miR-142-3p/*SLC7A11* ratio (expressed as MFI) in either CD25$^-$ (empty bars) or CD25$^+$ (filled bars) TCR-stimulated CD4$^+$ T cells upon the indicated EV treatments ($n = 7$ from six independent experiments). Data were analyzed by Friedman's test with Dunn's correction for multiple comparisons [(C), (D), and (H)], Spearman correlation (F), or *t* test (G). *$P < 0.05$; **$P < 0.01$; ***$P < 0.001$; ****$P < 0.0001$.

T_{reg}-EVs from pwRR-MS are functionally dysregulated and contain low amounts of miR-142-3p

Because robust experimental evidence has demonstrated T_{reg} cell dysfunction in people with relapsing-remitting multiple sclerosis (pwRR-MS) (*21*), we evaluated whether T_{reg}-EVs from pwRR-MS show aberrant immunosuppressive function, compared with those from healthy donors (HDs; fig. S7A and table S3). T_{reg}-EVs derived from pwRR-MS had completely lost their ability to dampen TCR-stimulated $CD4^+$ T cell proliferation and activation in vitro as compared with HD-derived T_{reg}-EVs (Fig. 6, A to C). Furthermore, compared with HD-derived T_{reg}-EVs, those from pwRR-MS were significantly less capable of lowering the amount of T-bet ($P < 0.0001$) and GATA3 ($P < 0.001$) (master regulators of the $CD4^+$ T_H1 and T_H2 cell lineages, respectively) in EV-target $CD4^+$ T cells (Fig. 6, D to F). T_{reg}-EVs from pwRR-MS were also significantly less efficient in curtailing the percentage of RORγt-expressing EV-target $CD4^+$ T cells ($P < 0.001$) (master regulator of the $CD4^+$ T_H17 lineage, highly relevant in MS pathogenic process) (Fig. 6, G and H).

Having identified miR-142-3p shuttled by EVs as an additional mediator of a healthy T_{reg} suppressive phenotype, we then decided to address its potential physiopathological relevance. To this aim, we analyzed the overall miRNA cargo of EVs released by either T_{conv} or T_{reg} cells isolated from pwRR-MS in comparison with those previously quantified in HD T_{conv}- and T_{reg}-EVs. A one-way analysis of variance (ANOVA) on miRNAs expressed in all samples ($n = 29$) indicated that the means of 19 of those 29 coexpressed miRNAs were significantly different ($P < 0.05$) among the four groups of samples, but only one miRNA (miR-142-3p) was found differentially expressed in HD compared with pwRR-MS T_{reg}-EVs, being markedly reduced in the latter (Fig. 6, I and J). This reduction was not simply mirroring a cell-based difference in miR-142-3p between HD and pwRR-MS T_{reg} cells because a two-way ANOVA analysis taking into account the compartment (intracellular versus EV associated) and the disease status (HD versus pwRR-MS) revealed that miR-142-3p had a higher expression in pwRR-MS compared with HD T_{reg} cells, suggesting a specific retention of that miRNA in the intracellular milieu of the diseased T_{reg} cells upon TCR stimulation (Fig. 6, K and L). The differential expression of miR-142-3p in T_{reg}-EVs was then validated in a larger cohort of HDs and pwRR-MS ($n = 9$ and $n = 18$, respectively; Fig. 6, M and N, fig. S7B) and confirmed by a multivariable logistic regression model correcting for age and gender and by absolute assessment through droplet digital PCR (fig. S7, C to E). Intriguingly, the impaired capability to shuttle miR-142-3p demonstrated by T_{reg} cells from pwRR-MS was also reported in the mouse system: In particular, T_{reg} cells isolated from mice with active EAE and cultured in vitro released EVs with significantly reduced amounts of miR-142-3p ($P < 0.0001$), compared with T_{reg} cells isolated from the healthy counterparts (fig. S7, F and G).

The ectopic increase in miR-142-3p cargo in T_{reg}-EVs by transfection of a mimic molecule was able to significantly ($P < 0.0001$) enhance their antiproliferative effect over TCR-stimulated $CD4^+$ T cells, supporting the direct involvement of this miRNA in suppressing those cells; furthermore, T_{conv}-EVs did also acquire an antiproliferative effect upon miR-142-3p transfection although not comparable with that of T_{reg}-EVs, suggesting not only the key relevance of this miRNA shuttling for the acquisition of immunosuppressive functions but also the importance of the overall molecular context in EVs (Fig. 6O). Moreover, miR-142-3p mimic transfection failed to rescue the antiproliferative effect of pwRR-MS T_{reg}-EVs over TCR-stimulated $CD4^+$ T cells, pointing to additional molecular defects associated with T_{reg}-EVs in pwRR-MS (Fig. 6O).

MiR-142-3p shuttled by T_{reg}-EVs marks disease severity in pwRR-MS

Because the quantity of miR-142-3p shuttled by T_{reg}-EVs (but not T_{conv}-EVs) was able to discriminate pwRR-MS from HDs [area under the receiver operating characteristic (ROC) curve; Fig. 7, A and B], we evaluated whether the actual amount of miR-142-3p shuttled by T_{reg}-EVs in pwRR-MS may have clinical relevance. To this aim, we estimated its correlation with anthropometric indexes [age, sex, and body mass index (BMI)] on the one side and with disease duration and parameters relative to disease severity [expanded disability status score (EDSS), number of relapses after disease onset, brain lesion load, and number of brain gadolinium-enhancing lesions] on the other. Although T_{reg}-EV–shuttled miR-142-3p did not correlate with age, disease duration, or BMI, it did inversely correlate with EDSS (Fig. 7, C to E), indicating that a reduced capability of T_{reg} cells to shuttle miR-142-3p through EVs is associated with increasing clinical disability. Furthermore, the amount of T_{reg}-EV–shuttled miR-142-3p was lower in active cases in pwRR-MS as compared with inactive ones, considering either the experience of relapse or the presence of gadolinium-enhancing lesions (Fig. 7F). In particular, low T_{reg}-EV–shuttled miR-142-3p amounts were detected in individuals having experienced one or more relapses within 6 months before blood collection compared with those with no relapses (Fig. 7G). Moreover, the quantity of miR-142-3p shuttled by T_{reg} cells through EVs inversely correlated ($P < 0.01$) with the number of brain gadolinium-enhancing lesions, revealing a direct association between the miR-142-3p shuttling capability of T_{reg} cells and inflammatory activity in patients' brains (Fig. 7H).

DISCUSSION

Extracellular miRNAs may revolutionize medical diagnostics, but whether they actually represent a distinct paradigm of intercellular signaling remains uncertain. Here, we demonstrate that miR-142-3p, an indispensable intrinsic regulator of T_{reg} cell homeostasis and suppressive capacity (*30*), is also prominently shuttled to bystander cells through EVs released by T_{reg} cells upon physiologically relevant TCR stimulatory signals in vitro (in both the human and mouse systems), becoming an antiproliferative message to those bystander T cells. This release of miR-142-3p–carrying EVs, therefore, represents a passive, noncompetitive, cell contact–independent suppressive mechanism (*31*). Although proliferation and function are traditionally perceived as separated in T_{reg} cells, we instead envision that the capability of a T_{reg} cell to engage anabolic growth and cell division (by also down-regulating miR-142-3p and, hence, relieving its inhibitory effects on mRNAs linked to cell proliferation) is intrinsically linked to the suppression of bystander target cells by shuttling miR-142-3p through EVs.

A prototypical example of this regulatory loop is given by *SLC7A11*. Upon TCR stimulation, the need for an efficient antioxidant network makes the up-regulation of this cystine/glutamate antiporter (critically involved in glutathione metabolism) a key factor in both proinflammatory and anti-inflammatory T cells (*29*, *32*, *33*). We recently found that defective *SLC7A11* induction in T_{reg} cells from pwRR-MS associates with their reduced proliferative potential

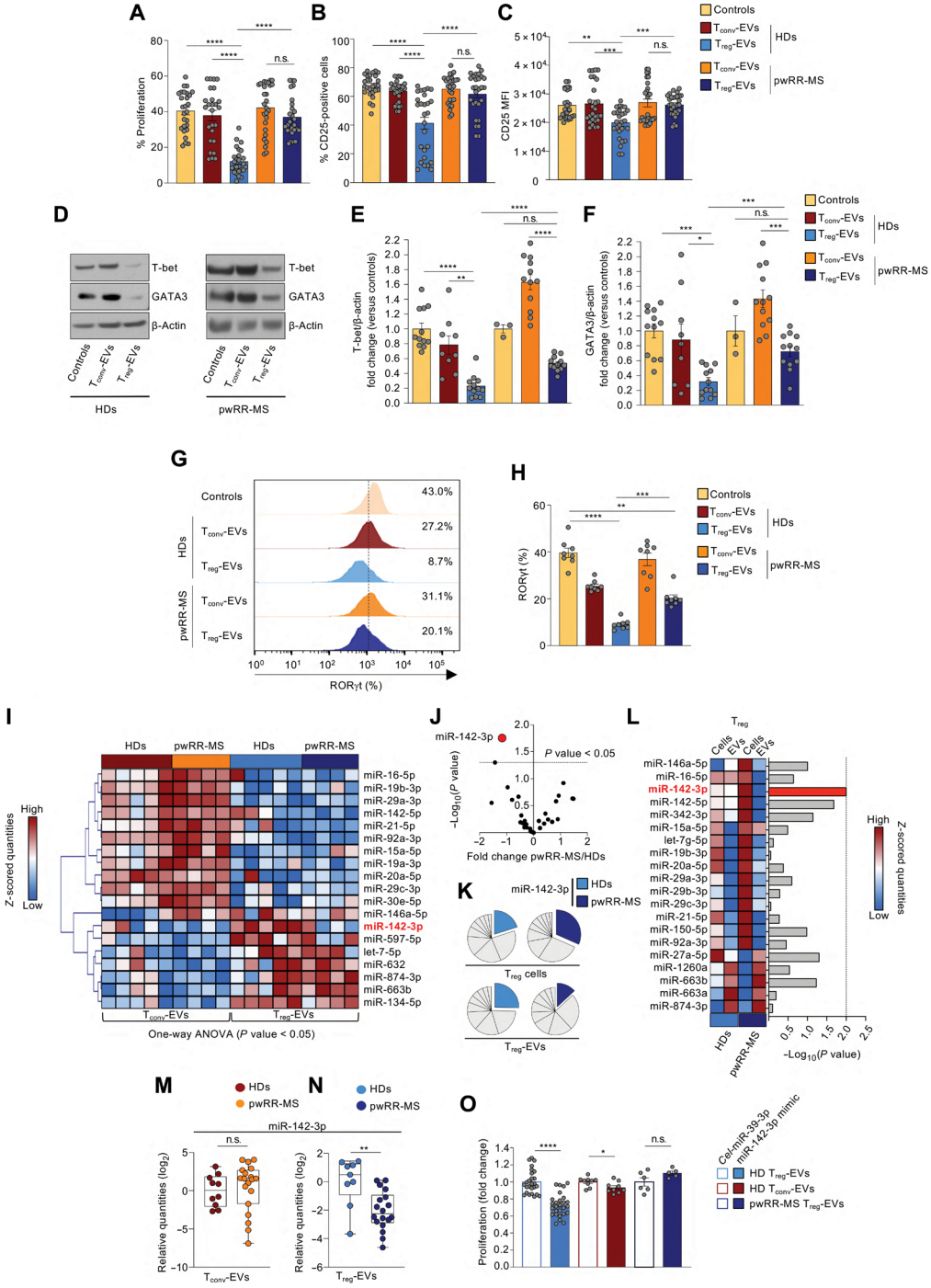

Fig. 6. T_{reg}-EVs from pwRR-MS are functionally impaired and shuttle a lower amount of miR-142-3p. (**A** to **C**) Bar graphs (means ± SEM with all experimental points, minimum $n = 26$ measurements from six independent experiments) showing the percentage of proliferating cells (assessed by flow cytometry in a CellTrace violet dilution assay) (A), the percentage of $CD25^+$ cells (B), and CD25 MFI (C) of TCR-stimulated $CD4^+$ T cells upon the indicated treatments. (**D** to **F**) Immunoblotting of T-bet and GATA3 [representative experiments, (D)] and bar graphs (means ± SEM with all experimental points) showing the relative normalized quantifications of T-bet (E) and GATA3 (F) protein abundance in TCR-stimulated $CD4^+$ T cells upon the indicated treatments. Data are from a minimum of $n = 9$ measurements from four independent experiments for HDs, $n = 12$ from two independent experiments for pwRR-MS, or $n = 3$ controls. (**G** and **H**) Representative experiment (G) and bar graph [means ± SEM with all experimental points, (H)] showing the percentage of RORγt-expressing cells as assessed by flow cytometry analysis of TCR-stimulated $CD4^+$ T cells treated as indicated ($n = 8$ from two independent experiments). (**I**) Heatmap showing miRNA hierarchical clustering based on the *z*-scored quantities of the 19 miRNAs identified as being significantly enriched ($P < 0.05$) in a one-way ANOVA test when comparing T_{reg}-EVs and T_{conv}-EVs from either HDs or pwRR-MS. (**J**) Volcano plot reporting the fold changes (*x* axis) and $-\log_{10}$ *P* values (*y* axis) for miRNA expression comparison between EVs released by T_{reg} cells from HDs versus pwRR-MS [groups as in (I)]. miR-142-3p, which is down-regulated in pwRR-MS-EVs with a *t* test $P < 0.05$, is highlighted in red in both (I) and (J). (**K**) Pie charts showing the mean differential quantitative representation of the first 10 most-expressed miRNAs in either T_{reg} cells (top) or T_{reg}-EVs (bottom) in HDs (left) and pwRR-MS (right, three donors per group); the differential ranking position of miR-142-3p in the different sample types is highlighted. (**L**) Heatmap showing the *z*-scored quantities of the 20 most-expressed miRNAs in the indicated samples; the bar graph on the right reports the $-\log_{10}$ *P* values as determined by a two-way ANOVA (compartment, intracellular versus EV associated; disease status, healthy versus pwRR-MS). The bar relative to miR-142-3p ($P < 0.01$) is highlighted in red. (**M** and **N**) Box and whisker plots (min to max with median and IQR, including all experimental points) showing miR-142-3p quantities (relative to U6 small nuclear RNA) in T_{conv}-EVs from an additional 10 HDs and 19 pwRR-MS (M) and T_{reg}-EVs from an additional 9 HDs and 18 pwRR-MS (N). (**O**) Bar graph (means ± SEM with all experimental points) showing the fold change in proliferation (assessed by flow cytometry in a CellTrace violet dilution assay) of TCR-stimulated $CD4^+$ T cells upon treatment with either healthy T_{reg}-EVs (minimum $n = 26$ from four independent experiments), healthy T_{conv}-EVs ($n = 9$ from two independent experiments), or T_{reg}-EVs from pwRR-MS (minimum $n = 5$ from two independent experiments) transfected with either *Cel*-miR-39-3p (used as control mimic) or miR-142-3p, as indicated. Data were analyzed by ordinary one-way ANOVA with Tukey's multiple comparisons test [(A) to (C)]; Kruskal-Wallis with Dunn's multiple comparisons within the different groups (HDs and pwRR-MS) [(E) and (F)]; Mann-Whitney between T_{reg}-EVs from HDs and pwRR-MS (for T-bet) and unpaired *t* (for GATA3); Kruskal-Wallis with Dunn's multiple comparisons within the different groups (HDs and pwRR-MS as compared with controls); Mann-Whitney only between T_{reg}-EVs from HDs and pwRR-MS (H); Mann-Whitney [(M) and (N)]; and unpaired *t* for HDs and Mann-Whitney for pwRR-MS (O). $^*P < 0.05$; $^{**}P < 0.01$; $^{***}P < 0.001$; $^{****}P < 0.0001$; n.s., not significant.

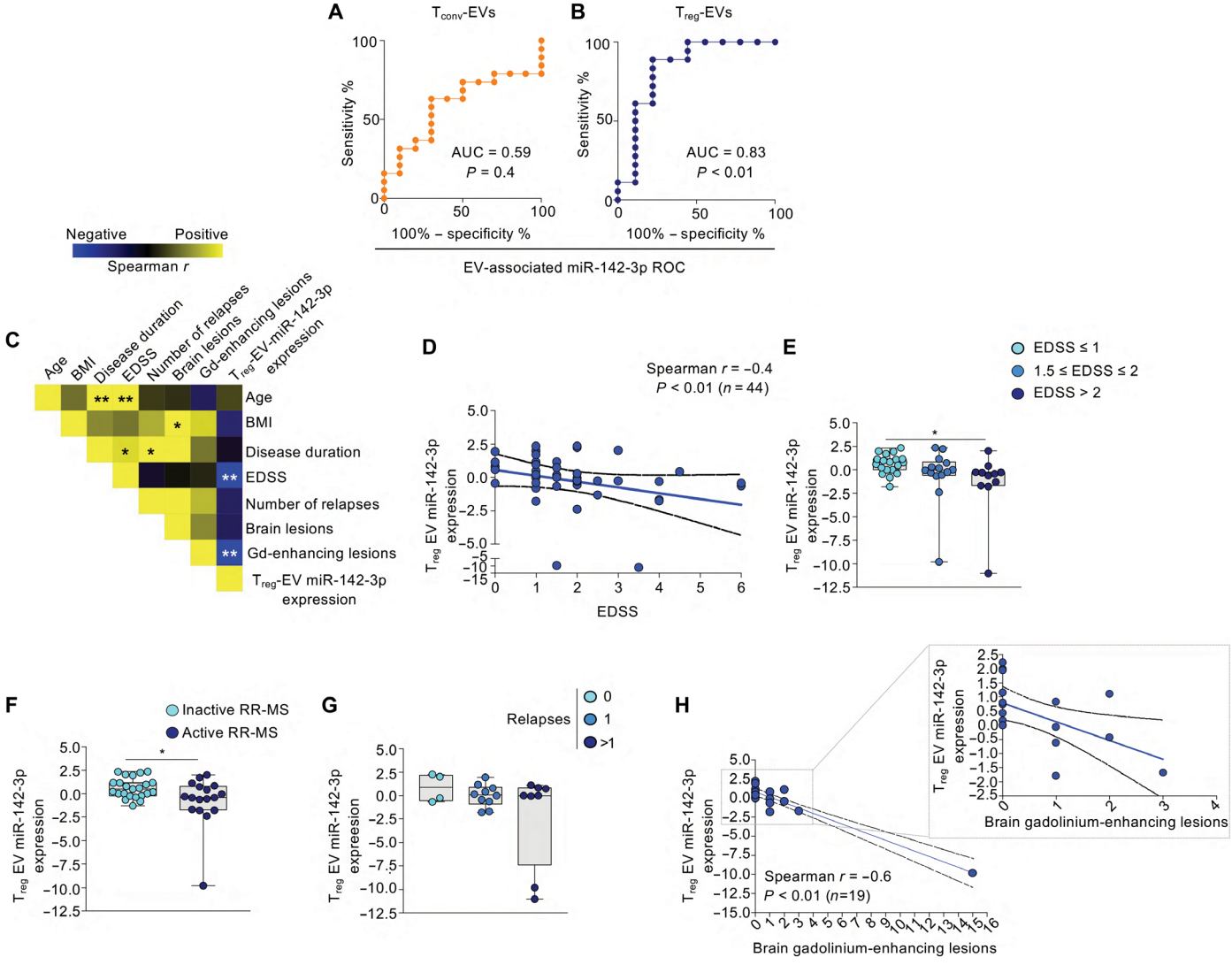

Fig. 7. The miR-142-3p content of T_{reg}-EVs from pwRR-MS inversely correlates with disease score and brain gadolinium-enhancing lesions. (**A** and **B**) ROC curves showing the capability of either T_{conv}-EV–shuttled (A) or T_{reg}-EV–shuttled (B) miR-142-3p to discriminate HDs from pwRR-MS; AUC and *P* values are also reported. (**C**) Heatmap showing the correlation matrix (yellow for positive, and blue for negative Spearman's rank; interval, −0.4 to +0.4) for the indicated anthropometric and disease-related parameters. (**D**) Scatter plot showing the linear correlation between the EDSS (*x* axis) and expression of T_{reg}-EV–shuttled miR-142-3p (*y* axis, normalized by the experimental mean) in the analyzed pwRR-MS samples ($n = 44$). Spearman *r* and *P* value are also reported; dashed lines indicate the 95% confidence interval. (**E** to **G**) Box and whisker plots (min to max with median and IQR, including all experimental points) showing miR-142-3p expression in T_{reg}-EVs from pwRR-MS stratified by EDSS (E), activity phase (F), and number of relapses (G). (**H**) Scatter plot showing the linear correlation between the number of brain gadolinium (Gd)–enhancing lesions (*x* axis) and expression of T_{reg}-EV–shuttled miR-142-3p (*y* axis) in the analyzed pwRR-MS ($n = 19$); in the zoomed-in box, only the pwRR-MS with EDSS < 4 are shown. Spearman *r* and *P* value are also reported; dashed lines indicate the 95% confidence interval. Data were analyzed by nonparametric Spearman correlation [(C), (D), and (H)], Kruskal-Wallis test with Dunn's correction for multiple comparisons [(E) and (G)], or Mann-Whitney test (F). $*P < 0.05$; $**P < 0.01$.

compared with healthy T_{reg} cells (*23*). The present work adds that this defect may be directly connected to higher T_{reg} intracellular retention of miR-142-3p in pwRR-MS, which leads to its reduced release and, consequently, decreased capability to inhibit *SLC7A11* expression in paracrine target T cells (fig. S8A). This loop may play a particularly relevant role in pwRR-MS, where the unbalanced activity of this protein channel is known to fuel unrestrained immune cell proliferation, inflammation, and brain dysfunction (*34*, *35*).

The recognition that, during the course of an immune response, the information can be transferred from one cell type to another in the form of RNA molecules actually dates back to around 50 years ago (*36*–*38*). Nonetheless, only in the past 2 decades have we abandoned the idea of a labile RNA and fully recognized that extracellular RNA-based communication, mostly based on a sophisticated EV containment, is an ancient, powerful, and universal code for cells to influence each other (*39*, *40*). The growing knowledge on the mechanisms beyond this code is opening unprecedented therapeutic opportunities (*41*). In particular, initial observations of the beneficial effects of T_{reg}-EVs on the hyperinflammatory response linked to transplant rejection point to their potential use as

an alternative to immune-modulatory T_{reg} cell–based therapies (*18*, *42*). Because EVs are expected to remain biologically stable in different contexts, being unable to either replicate or transdifferentiate (*43*), they would overcome the pitfalls relative to cell plasticity, which undermine T_{reg} cell immunosuppressive capacity upon in vivo infusion (*44*, *45*). Although the beneficial, albeit limited, effect of healthy T_{reg}-EVs in the EAE mouse system calls for further studies aimed at optimizing EV dose and administration route, the failed functional rescue of dysfunctional pwRR-MS T_{reg}-EVs by the ectopic enhancement of their miR-142-3p cargo, shown here, may suggest the need for therapies based on T_{reg}-EVs from allogeneic HDs.

This study unveiled the clinical relevance of an EV-based mechanism of T_{reg} cell function, supported by the correlation between the reduced capability of T_{reg} cells to shuttle miR-142-3p through EVs and the presence and number of brain gadolinium-enhancing lesions on magnetic resonance imaging, the most specific indicator of ongoing inflammatory activity within the CNS of pwRR-MS. This correlation not only underscores the potential role of the identified mechanism in pwRR-MS pathogenesis but also highlights its prospect as a biomarker for monitoring disease activity (fig. S8B).

Our study has some limitations. The mechanisms underlying EV biogenesis and cargo selection on the EV cell source side and EV uptake and intracellular fate of its molecular content on the EV target cell side have not been characterized yet. In particular, the cellular and molecular defects that lead to an impaired release of EV-associated miR-142-3p (but not other miRNAs) remain undefined. A second limitation is relative to the in vivo experiments; although intraperitoneal administration of the EVs in the EAE animal model was chosen on the basis of the hypothesis that a systemic distribution is beneficial, we do not know whether other routes (or different doses or timing of T_{reg}-EV injections) may be more efficacious. Specifically, it would be relevant to test the intrathecal administration of T_{reg}-EVs, which may bring them directly to the actual disease site. Furthermore, we did not track the EVs in vivo and, hence, are still unable to define their stability, the preferential target tissues and cells (in particular, whether the EVs were able to pass the blood-brain barrier), and the mechanism of action in the organism. Regarding the dysregulated molecular phenotype and function of T_{reg}-EVs in pwRR-MS, at the moment, we are unaware of whether the previously unknown phenomenon described here may be present also in other autoimmune disorders or is only linked to multiple sclerosis. Last, the report of a correlation between the miR-142-3p content of T_{reg}-EVs in pwRR-MS and their ongoing inflammatory activity within the CNS is clinically relevant; nonetheless, the use of T_{reg}-EVs as biomarkers of disease status will require rigorous validation and standardization, which remains an ongoing challenge.

In conclusion, we propose that T_{reg} cell–shuttled miR-142-3p, stabilized by EV protection, may help curb the adaptive effector response at the paracrine, but possibly also at the endocrine, level and can maintain immune tolerance in mammalian physiological conditions. This route of signal transmission also represents a distinct pathogenic mechanism contributing to the breach of immune homeostasis in pwRR-MS. Knowledge of this defect in T_{reg} function may drive the design of treatments aimed at restoring T_{reg} cell function in pwRR-MS and other autoimmune diseases.

MATERIALS AND METHODS

Study design

This study was first designed to investigate the role of EVs released by human T_{reg} cells in the control of $CD4^+$ T cell function. To this aim, we performed in vitro studies, treating TCR-stimulated $CD4^+$ T cells with T_{reg}-EVs and assessing their effect on cell proliferation, activation, and polarization. We also traced the molecular mechanism of this effect by linking a specific miRNA to gene expression modulation in T_{reg}-EV target $CD4^+$ T cells. To expand these observations in vivo, we evaluated the effect of T_{reg}-EVs on disease progression, lymphocyte infiltration into the CNS, and systemic inflammation in EAE mice. The pathogenic implication of this biological system was studied by analyzing the dysregulated molecular phenotype and function of T_{reg}-EVs from pwRR-MS. The sample size of the human cohort was chosen on the basis of similar studies in the literature, and experiments were always performed in technical and independent biological replicates (the precise number is specified in the figure legends).

All of the experimental procedures on mice were approved by the Institutional Animal Care at the Università degli Studi di Napoli "Federico II" (Italy). The mice were randomly assigned to different experimental groups; moreover, both the investigators following the disease course and the pathologist analyzing the relative histology were blinded to the treatment assignment of the mice. The analysis of human samples was approved by the Institutional Review Board of Università degli Studi di Napoli Federico II and Università degli Studi di Milano-Bicocca, Monza (Italy) and was conducted in accordance with the Declaration of Helsinki; all participants signed a written informed consent. Specifically, we obtained peripheral blood mononuclear cells (PBMCs) from HDs ($n = 48$, with no history of inflammatory, endocrine, or autoimmune disease) and pwRR-MS ($n = 72$, table S3). pwRR-MS were stratified as being in either an active or an inactive phase of the disease on the basis of the experience of relapse, the presence of gadolinium-enhancing lesions, or both within 6 months before blood collection.

Human primary $CD4^+$ T cells

Total $CD4^+$ T cells, T_{conv} cells ($CD4^+CD25^-$), and T_{reg} cells ($CD4^+CD25^{hi}$) were isolated from PBMCs by magnetic cell separation with the Dynabeads regulatory $CD4^+CD25^+$T Cell Kit (Invitrogen) or by high-performance cell sorting (BD FACSAria II) after staining with the following antibodies with a 1:100 dilution: allophycocyanin (APC) anti-human CD127 (Miltenyi Biotec, REA614), phycoerythrin-cyanine7 (PE-Cy7) mouse anti-human CD25 (BD Biosciences, M-A251), and APC-H7 mouse anti-human CD4 (BD Pharmingen, RPA-T4) (*21*). T_{reg} cell purity was checked by anti-Human FoxP3 Staining Kit (BD Biosciences), following the manufacturer's protocol; purity data were acquired by BD LSRFortessa (BD Biosciences) and analyzed with FlowJo software version 10.7. All primary T cells were cultured (1×10^6 cells/ml) in AIMV medium (Gibco) and TCR-stimulated with anti-CD3 and anti-CD28-coated Dynabeads (0.2 beads per cell, to mimic physiological in vivo activating conditions) (Invitrogen) (*46*, *47*). $CD4^+$ T cell proliferation was measured by fluorescent CellTrace violet (5 nM) dilution assay (Thermo Fischer Scientific) according to the manufacturer's instructions. Caspase activation was measured by the CellEvent Caspase-3/7 Green Flow Cytometry Assay Kit (Life Technologies). For both proliferation and cell death, samples were acquired by a BD

FACSCanto II (BD Biosciences), and data were analyzed with FlowJo software version 10.7.

Cell lines

Jurkat cells were cultured (3×10^5 cells/ml) in RPMI 1640 medium supplemented with 10% fetal bovine serum (FBS), 1% penicillin-streptomycin, and 1% L-glutamine. HEK-293 cells were obtained from American Type Culture Collection and were cultured in Dulbecco's modified Eagle's medium supplemented with 10% (v/v) FBS and 1% penicillin/streptomycin (Gibco). All of the cultures were maintained at 37°C in a 5% CO_2-humidified atmosphere.

EV isolation, transfection, and treatment

EVs were isolated from conditioned medium of TCR-stimulated T_{conv} and T_{reg} cells (upon 72 hours of culturing) or from unconditioned medium (controls) using Exo-spin columns (Cell Guidance) according to the manufacturer's protocol or by differential centrifugation and then characterized for size and morphology (see the Supplementary Materials). Isolated EVs were transfected using an Exo-Fect siRNA/miRNA Transfection kit (System Biosciences, according to the manufacturer's instructions) with (i) scramble Cy3-labeled control siRNA scramble (10 μM), (ii) AF488-conjugated miR-142-3p mimic (67 μM) (System Biosciences), or (iii) hsa-miR-142-3p or *Caenorhabditis elegans* miR-39-3p (67 μM) (*Cel*-miR-39-3p, negative control) miRCURY LNA miRNA Mimic (100 nM, QIAGEN). For EV treatment, $CD4^+$ T cell–derived isolated EVs (or mock EVs, as controls) were used to treat heterologous $CD4^+$ T cells (or Jurkat cells), in combination with TCR stimulation (as described above) for either 24, 48, or 72 hours, depending on the downstream assay, at a ratio of EV-releasing to EV-recipient cells of 1:1 (unless otherwise specified).

Real-time qPCR

EV-associated miRNAs were extracted using a miRNeasy Serum/Plasma advanced kit (QIAGEN) according to the manufacturer's protocol in the presence of MS2 carrier RNA (Roche) and synthetic RNA spike-in resembling miRNAs (UniSp2, UniSp4, and UniSp5) to monitor for RNA isolation efficiency and reproducibility. A fixed volume of EV-miRNA extract was used as reverse transcription input using miRCURY-LNA RT Kit (QIAGEN) according to the manufacturer's instructions; this approach was preferred to a fixed quantity of RNA because the EV-RNA yield is too low to be accurately measured. *Cel*-miR-39-3p was added as cDNA synthesis control. Total RNA was instead extracted from cells using the RNAqueous Total RNA Isolation Kit (Ambion) or by the Cells-to-CT 1-Step Power SYBR Green Kit (Invitrogen, designed for samples with extremely low number of cells).

Luciferase assay

The two putative miR-142-3p binding sites were separately cloned into the pmirGLO luciferase vector (Promega), and, as controls, oligonucleotides containing a mutated seed region were also designed (table S4). Transfection of HEK-293 cells with luciferase vectors and synthetic miRNA mimics (miRCURY LNA, QIAGEN) was then performed using Lipofectamine LTX Transfection Reagent (Thermo Fisher Scientific) following the manufacturer's instructions. Luciferase assays were performed as previously described (*48*). The data generated were expressed as relative luciferase expression, after normalization to the *Renilla* luciferase reporter, contained in the pmirGLO vector, and used as an internal control.

Proteomics and transcriptomics

Proteins were analyzed by liquid chromatography combined with tandem mass spectrometry (MS/MS). All raw files were processed by the SEQUEST HT algorithm in Proteome Discoverer 2.5 software (Thermo Fisher Scientific). Experimental MS/MS spectra were compared with the in silico–digested *H. sapiens* protein database (UniProt, September 2022) using previously reported search criteria and normalization methods (*49*). For transcriptomics, total RNA (100 ng) was mRNA enriched using the oligo(dT) bead system and enzymatically fragmented; then, library preparation was performed using a TruSeq Stranded mRNA Sample preparation kit (Illumina Inc.). The details for these techniques can be found in the Supplementary Materials.

Immunoblotting

Proteins were separated onto NuPAGE 4 to 12% bis-tris precast gels (Invitrogen) and transferred onto nitrocellulose filter membranes (Amersham Protran, Cytiva), which were blocked in 5% nonfat milk in phosphate-buffered saline 0.05% Tween 20 for 2 hours and then incubated overnight with the following antibodies: rabbit anti-human pS6 ($Ser^{235/236}$, D57.2.2E, Cell Signaling Technologies), mouse anti-human S6 (54D2, Cell Signaling Technologies), rabbit anti-human pLat (Tyr^{220}, Cell Signaling Technologies), Lat (E3S5L and E3U6J, respectively, Cell Signaling Technologies), rabbit anti-human p27 Kip1 (D69C12, Cell Signaling Technologies), rabbit anti-human T-bet/TBX21 (D6N8B, Cell Signaling Technologies), rabbit anti-human GATA3 (D13C9, Cell Signaling Technologies), rabbit anti-human xCT/SLC7A11 (D2M7A, Cell Signaling Technologies), mouse anti-human p-ERK (E-4, Santa Cruz Biotechnology), rabbit anti-human Erk (K23, Santa Cruz Biotechnology), and goat anti-human actin (I-19, Santa Cruz Biotechnology). All filters were quantified by densitometric analysis of the bands using the program ImageJ 1.47. All antibodies used are listed in table S5, and uncropped images relative to immunoblotting results are reported in fig. S9.

Flow cytometry

$CD4^+$ T cells were stained with the following antibodies for surface markers: APC-H7 mouse anti-human CD4 (RPA-T4, BD Biosciences), BUV395 mouse anti-human CD3 (SK7, BD Biosciences), BB700 mouse anti-human CD134 (ACT35, BD Biosciences), BB700 mouse anti-human CD69 (FN50, BD Biosciences), PE-Cy7 mouse anti-human CD25 (M-A251, BD Biosciences), APC rat anti-human RORγt (AFKJS-9, eBioscience), PE rat anti-human FoxP3 (PCH101 eBioscience), fluorescein isothiocyanate (FITC) mouse anti-human T-bet (4B10, BioLegend), and BV421 mouse anti-human GATA3 (L50-823, BD Pharmingen).

For mouse cells, CNS cellular suspensions were loaded over a Percoll (Merck) gradient (37 to 70%) to isolate mononuclear cells at the interphase and stained with the following antibodies: purified rat anti-mouse CD16/CD32 (2.4G2, BD Pharmingen), FITC rat anti-mouse CD45 (30-F11, BD Pharmingen), Alexa Fluor 700 rat anti-mouse CD4 (RM-45, BD Pharmingen), BUV496 rat anti-mouse B220 (RA3-6B2, BD Pharmingen), BV605 rat anti-mouse Ly6C (AL-21, BD Pharmingen), BV650 rat anti-mouse Ly6G (1A8, BD Pharmingen), peridinin-chlorophyll-protein (PerCP)–Cy5.5

hamster anti-mouse CD195 (HM-CCR5, BioLegend), PE-Cy7 rat anti-mouse CD11b (M1/70, BioLegend), APC rat anti-mouse CD25 (PC-61, BD Pharmingen), APC-Cy7 rat anti-mouse CD4 (GK1.5, BD Pharmingen), BB515 rat anti-mouse CD195/CCR5 (C34-3448, BD Pharmingen), PE rat anti-mouse FoxP3 (FJK-16s, Invitrogen), PE-Cy7 rat anti-mouse CD11b (M1/70, BioLegend), and Pacific Blue rat anti-mouse Ly6G (1A8, BioLegend). All samples were acquired by BD FACSCanto II (BD Biosciences) or Cytoflex-LX Flow Cytometer. Data were analyzed with FlowJo software version 10.7.

For the PrimeFlow RNA assay, concomitant single-cell–based expression of activation markers, miR-142-3p, and *SLC7A11* mRNA was performed by treating EV-treated $CD4^+$ T cells with fixable viability dye for 30 min at 4°C, then washing, and staining them for surface (PE-Cy7 CD25) and intracellular (PE FoxP3, PCH101) markers; in sequence, the PrimeFlow RNA assay was performed for SLC7A11 mRNA (VA1-3007681-PF, high-sensitivity design) and then hsa-miR-142-3p (VA4-3102286-PF) according to the manufacturer's instructions (Affymetrix). Samples were acquired by BD FACSCanto II (BD Biosciences), and data were analyzed with FlowJo software version 10.7. All antibodies used are listed in table S5.

Cytokine measurement

$CD4^+$ T cells were evaluated for cytokine production by Luminex technology, using a bead-based multianalyte immunoassay (customized T_H1/T_H2/T_H9/T_H17/T_H22/T_{reg} 18-Plex panel, Thermo Fisher Scientific). Assays were conducted according to the manufacturer's recommendations. xPONENT 3.1 software (Luminex 200) was used for data acquisition.

Statistical analysis

Individual-level data are presented in data file S5. Comparisons between groups (in both ex vivo and in vitro experiments) were performed by either unpaired Student's *t* test or nonparametric Mann-Whitney test (for two groups) and by ANOVA or Kruskal-Wallis (for three or more groups) for normally and nonnormally distributed variables, respectively, followed by correction for multiple hypothesis testing (Šidák's, Holm-Šidák's, or Tukey's correction for ANOVA and Dunn's correction for Kruskal-Wallis) or Friedman's test with Dunn's correction for nonparametric matched measurements. Multivariate unconditional logistic regression model was performed to assess the independent contribution of miR-142-3p, age, and gender in the prediction of MS; odds ratios and 95% confidence intervals were calculated. ROC curve for the multivariate model was drawn and the corresponding area under the curve (AUC) was calculated. The correlation scores were assessed by Spearman correlation coefficient and graphically represented along with the regression line and 95% confidence bands. Analyses were performed with SAS Software 9.4 or GraphPad Prism 9.0. $P < 0.05$ was considered statistically significant.

For omics data analysis, starting from the list of experimentally identified proteins and transcripts, the corresponding human protein-protein interaction (PPI) network was extracted. By means of the STRING Cytoscape APP (*50*), known PPI interactions were retrieved by considering only edges characterized by an "experiments" or "database" score > 0.15 (*51*). Both STRING and Cytoscape BINGO APPs (*52*) were used for evaluating the most represented *H. sapiens* Gene Ontology (GO) terms; hypergeometric test, Benjamini-Hochberg false discovery rate (FDR) correction, and a significance level ≤ 0.05 were applied to select the most-represented GO terms by BINGO; default parameters were used for STRING. The lists of differentially expressed genes were also screened with the DAVID 6.7 Functional Annotation Tool (*53*) to highlight overrepresented biological themes for each considered contrast using the *H. sapiens* genome as a customized population background. Fold enrichment was considered if Fisher's exact *P* value was equal to or smaller than 0.01 (or exact *P* value was equal to or smaller than 0.05), and the minimum number of genes was set to 2.

For GSEA, we first obtained the list of targets (targetome) of the miRNAs of interest using the experimentally validated miRNA-target interactions reported by miRTarBase (*54*). Then, for each miRNA, we applied GSEA v4.2.3 (Broad Institute) (*55*) to evaluate the distribution of the targetome across the ranked list of expressed genes ordered by the fold change of the comparison of T_{reg}-EV– versus control-treated $CD4^+$ T cells. By running the leading edge analysis, we extracted the subset of core genes contributing mostly to the enrichment of the targetome in one of the ends of the ranked list. Each leading-edge gene was then characterized by a running ES (the ES at this point in the ranked list of genes) and a core score (representing the enrichment *P* value of that gene).

Supplementary Materials

The PDF file includes:
Materials and Methods
Figs. S1 to S9
Tables S1 to S5
Legends for data files S1 to S5
References (*56*–*61*)

Other Supplementary Material for this manuscript includes the following:
Data files S1 to S5
MDAR Reproducibility Checklist

REFERENCES AND NOTES

1. Y. Couch, E. I. Buzàs, D. Di Vizio, Y. S. Gho, P. Harrison, A. F. Hill, J. Lötvall, G. Raposo, P. D. Stahl, C. Théry, K. W. Witwer, D. R. F. Carter, A brief history of nearly EV-erything–The rise and rise of extracellular vesicles. *J. Extracell. Vesicles* **10**, e12144 (2021).
2. S. G. van der Grein, K. A. Y. Defourny, E. F. J. Slot, E. N. M. Nolte-'t Hoen, Intricate relationships between naked viruses and extracellular vesicles in the crosstalk between pathogen and host. *Semin. Immunopathol.* **40**, 491–504 (2018).
3. V. Estévez-Souto, S. Da Silva-Álvarez, M. Collado, The role of extracellular vesicles in cellular senescence. *FEBS J.* **290**, 1203–1211 (2023).
4. A. Picca, F. Guerra, R. Calvani, H. J. Coelho-Júnior, F. Landi, R. Bernabei, R. Romano, C. Bucci, E. Marzetti, Extracellular vesicles and damage-associated molecular patterns: A Pandora's box in health and disease. *Front. Immunol.* **11**, 601740 (2020).
5. E. I. Buzas, The roles of extracellular vesicles in the immune system. *Nat. Rev. Immunol.* **23**, 236–250 (2022).
6. M. Mittelbrunn, C. Gutiérrez-Vázquez, C. Villarroya-Beltri, S. González, F. Sánchez-Cabo, M. Á. González, A. Bernad, F. Sánchez-Madrid, Unidirectional transfer of microRNA-loaded exosomes from T cells to antigen-presenting cells. *Nat. Commun.* **2**, 282 (2011).
7. D. G. Saliba, P. F. Céspedes-Donoso, Š. Bálint, E. B. Compeer, K. Korobchevskaya, S. Valvo, V. Mayya, A. Kvalvaag, Y. Peng, T. Dong, M.-L. Tognoli, E. O'Neill, S. Bonham, R. Fischer, B. M. Kessler, M. L. Dustin, Composition and structure of synaptic ectosomes exporting antigen receptor linked to functional CD40 ligand from helper T cells. *eLife* **8**, e47528 (2019).
8. K. Choudhuri, J. Llodrá, E. W. Roth, J. Tsai, S. Gordo, K. W. Wucherpfennig, L. C. Kam, D. L. Stokes, M. L. Dustin, Polarized release of T-cell-receptor-enriched microvesicles at the immunological synapse. *Nature* **507**, 118–123 (2014).
9. P. F. Céspedes, A. Jainarayanan, L. Fernández-Messina, S. Valvo, D. G. Saliba, E. Kurz, A. Kvalvaag, L. Chen, C. Ganskow, H. Colin-York, M. Fritzsche, Y. Peng, T. Dong, E. Johnson, J. A. Siller-Farfán, O. Dushek, E. Sezgin, B. Peacock, A. Law, D. Aubert, S. Engledow, M. Attar, S. Hester, R. Fischer, F. Sánchez-Madrid, M. L. Dustin, T-cell trans-synaptic vesicles are distinct and carry greater effector content than constitutive extracellular vesicles. *Nat. Commun.* **13**, 3460 (2022).
10. L. Fernández-Messina, A. Rodríguez-Galán, V. G. de Yébenes, C. Gutiérrez-Vázquez, S. Tenreiro, M. C. Seabra, A. R. Ramiro, F. Sánchez-Madrid, Transfer of extracellular

vesicle-microRNA controls germinal center reaction and antibody production. *EMBO Rep.* **21**, e48925 (2020).
11. P. de Candia, C. Procaccini, C. Russo, M. T. Lepore, G. Matarese, Regulatory T cells as metabolic sensors. *Immunity* **55**, 1981–1992 (2022).
12. S. Sakaguchi, N. Sakaguchi, J. Shimizu, S. Yamazaki, T. Sakihama, M. Itoh, Y. Kuniyasu, T. Nomura, M. Toda, T. Takahashi, Immunologic tolerance maintained by $CD25^+$ $CD4^+$ regulatory T cells: Their common role in controlling autoimmunity, tumor immunity, and transplantation tolerance. *Immunol. Rev.* **182**, 18–32 (2001).
13. L. A. Smyth, K. Ratnasothy, J. Y. Tsang, D. Boardman, A. Warley, R. Lechler, G. Lombardi, CD73 expression on extracellular vesicles derived from $CD4^+$ $CD25^+$ $Foxp3^+$ T cells contributes to their regulatory function. *Eur. J. Immunol.* **43**, 2430–2440 (2013).
14. I. S. Okoye, S. M. Coomes, V. S. Pelly, S. Czieso, V. Papayannopoulos, T. Tolmachova, M. C. Seabra, M. S. Wilson, MicroRNA-containing T-regulatory-cell-derived exosomes suppress pathogenic T helper 1 cells. *Immunity* **41**, 89–103 (2014).
15. S. L. Tung, D. A. Boardman, M. Sen, M. Letizia, Q. Peng, N. Cianci, L. Dioni, L. M. Carlin, R. Lechler, V. Bollati, G. Lombardi, L. A. Smyth, Regulatory T cell-derived extracellular vesicles modify dendritic cell function. *Sci. Rep.* **8**, 6065 (2018).
16. M. Campos-Mora, J. De Solminihac, C. Rojas, C. Padilla, M. Kurte, R. Pacheco, T. Kaehne, Ú. Wyneken, K. Pino-Lagos, Neuropilin-1 is present on Foxp3+ T regulatory cell-derived small extracellular vesicles and mediates immunity against skin transplantation. *J. Extracell. Vesicles* **11**, e12237 (2022).
17. A. Torri, D. Carpi, E. Bulgheroni, M. C. Crosti, M. Moro, P. Gruarin, R. L. Rossi, G. Rossetti, D. Di Vizio, M. Hoxha, V. Bollati, C. Gagliani, C. Tacchetti, M. Paroni, J. Geginat, L. Corti, L. Venegoni, E. Berti, M. Pagani, G. Matarese, S. Abrignani, P. de Candia, Extracellular microRNA signature of human helper T cell subsets in health and autoimmunity. *J. Biol. Chem.* **292**, 2903–2915 (2017).
18. S. L. Tung, G. Fanelli, R. I. Matthews, J. Bazoer, M. Letizia, G. Vizcay-Barrena, F. N. Faruqu, C. Philippeos, R. Hannen, K. T. Al-Jamal, G. Lombardi, L. A. Smyth, Regulatory T cell extracellular vesicles modify T-effector cell cytokine production and protect against human skin allograft damage. *Front. Cell Dev. Biol.* **8**, 317 (2020).
19. A. D. Thome, J. R. Thonhoff, W. Zhao, A. Faridar, J. Wang, D. R. Beers, S. H. Appel, Extracellular vesicles derived from ex vivo expanded regulatory T cells modulate in vitro and in vivo inflammation. *Front. Immunol.* **13**, 875825 (2022).
20. K. Venken, N. Hellings, T. Broekmans, K. Hensen, J.-L. Rummens, P. Stinissen, Natural naive $CD4^+CD25^+CD127^{low}$ regulatory T cell (T_{reg}) development and function are disturbed in multiple sclerosis patients: Recovery of memory T_{reg} homeostasis during disease progression. *J. Immunol.* **180**, 6411–6420 (2008).
21. F. Carbone, V. De Rosa, P. B. Carrieri, S. Montella, D. Bruzzese, A. Porcellini, C. Procaccini, A. La Cava, G. Matarese, Regulatory T cell proliferative potential is impaired in human autoimmune disease. *Nat. Med.* **20**, 69–74 (2014).
22. V. Viglietta, C. Baecher-Allan, H. L. Weiner, D. A. Hafler, Loss of functional suppression by $CD4^+CD25^+$ regulatory T cells in patients with multiple sclerosis. *J. Exp. Med.* **199**, 971–979 (2004).
23. C. Procaccini, S. Garavelli, F. Carbone, D. Di Silvestre, C. La Rocca, D. Greco, A. Colamatteo, M. T. Lepore, C. Russo, G. De Rosa, D. Faicchia, F. Prattichizzo, S. Grossi, P. Campomenosi, F. Buttari, P. Mauri, A. Uccelli, M. Salvetti, V. Brescia Morra, D. Vella, M. Galgani, M. Mottola, B. Zuccarelli, R. Lanzillo, G. T. Maniscalco, D. Centonze, P. de Candia, G. Matarese, Signals of pseudo-starvation unveil the amino acid transporter SLC7A11 as key determinant in the control of T_{reg} cell proliferative potential. *Immunity* **54**, 1543–1560.e6 (2021).
24. D. Di Silvestre, S. Garavelli, C. Procaccini, F. Prattichizzo, G. Passignani, V. De Rosa, P. Mauri, G. Matarese, P. de Candia, $CD4^+$ T-cell activation prompts suppressive function by extracellular vesicle-associated MicroRNAs. *Front. Cell Dev. Biol.* **9**, 753884 (2021).
25. M. Catalano, L. O'Driscoll, Inhibiting extracellular vesicles formation and release: A review of EV inhibitors. *J. Extracell. Vesicles* **9**, 1703244 (2020).
26. P. de Candia, A. Torri, T. Gorletta, M. Fedeli, E. Bulgheroni, C. Cheroni, F. Marabita, M. Crosti, M. Moro, E. Pariani, L. Romanò, S. Esposito, F. Mosca, G. Rossetti, R. L. Rossi, J. Geginat, G. Casorati, P. Dellabona, M. Pagani, S. Abrignani, Intracellular modulation, extracellular disposal and serum increase of MiR-150 mark lymphocyte activation. *PLOS ONE* **8**, e75348 (2013).
27. R. R. Voskuhl, A. MacKenzie-Graham, Chronic experimental autoimmune encephalomyelitis is an excellent model to study neuroaxonal degeneration in multiple sclerosis. *Front. Mol. Neurosci.* **15**, 1024058 (2022).
28. X. Wang, H. Luo, H. Chen, W. Duguid, J. Wu, Role of proteasomes in T cell activation and proliferation. *J. Immunol.* **160**, 788–801 (1998).
29. P. J. Siska, B. Kim, X. Ji, M. D. Hoeksema, P. P. Massion, K. E. Beckermann, J. Wu, J. T. Chi, J. Hong, J. C. Rathmell, Fluorescence-based measurement of cystine uptake through xCT shows requirement for ROS detoxification in activated lymphocytes. *J. Immunol. Methods* **438**, 51–58 (2016).
30. W. L. Wang, C. Ouyang, N. M. Graham, Y. Zhang, K. Cassady, E. Y. Reyes, M. Xiong, A. M. Davis, K. Tang, D. Zeng, M. P. Boldin, microRNA-142 guards against autoimmunity by controlling T_{reg} cell homeostasis and function. *PLoS Biol.* **20**, e3001552 (2022).
31. B. Akkaya, E. M. Shevach, Regulatory T cells: Master thieves of the immune system. *Cell. Immunol.* **355**, 104160 (2020).
32. S. K. Garg, Z. Yan, V. Vitvitsky, R. Banerjee, Differential dependence on cysteine from transsulfuration versus transport during T cell activation. *Antioxid. Redox Signal.* **15**, 39–47 (2011).
33. T. B. Levring, A. K. Hansen, B. L. Nielsen, M. Kongsbak, M. R. von Essen, A. Woetmann, N. Ødum, C. M. Bonefeld, C. Geisler, Activated human $CD4^+$ T cells express transporters for both cysteine and cystine. *Sci. Rep.* **2**, 266 (2012).
34. O. Pampliega, M. Domercq, F. N. Soria, P. Villoslada, A. Rodriguez-Antiguedad, C. Matute, Increased expression of cystine/glutamate antiporter in multiple sclerosis. *J. Neuroinflammation* **8**, 63 (2011).
35. A. Martin, N. Vazquez-Villoldo, V. Gomez-Vallejo, D. Padro, F. N. Soria, B. Szczupak, S. Plaza-Garcia, A. Arrieta, T. Reese, J. Llop, M. Domercq, C. Matute, In vivo imaging of system xc- as a novel approach to monitor multiple sclerosis. *Eur. J. Nucl. Med. Mol. Imaging* **43**, 1124–1138 (2016).
36. H. Friedman, RNA in the immune response. Introductory remarks. *Ann. N. Y. Acad. Sci.* **207**, 5–7 (1973).
37. M. Stroun, P. Anker, M. Beljanski, J. Henri, C. Lederrey, M. Ojha, P. A. Maurice, Presence of RNA in the nucleoprotein complex spontaneously released by human lymphocytes and frog auricles in culture. *Cancer Res.* **38**, 3546–3554 (1978).
38. P. Anker, D. Jachertz, M. Stroun, R. Brogger, C. Lederrey, J. Henri, P. A. Maurice, The role of extracellular DNA in the transfer of information from T to B human lymphocytes in the course of an immune response. *J. Immunogenet.* **7**, 475–481 (1980).
39. M. Knip, M. E. Constantin, H. Thordal-Christensen, Trans-kingdom cross-talk: Small RNAs on the move. *PLOS Genet.* **10**, e1004602 (2014).
40. P. de Candia, V. De Rosa, M. Casiraghi, G. Matarese, Extracellular RNAs: A secret arm of immune system regulation. *J. Biol. Chem.* **291**, 7221–7228 (2016).
41. C. Fusco, G. De Rosa, I. Spatocco, E. Vitiello, C. Procaccini, C. Frigè, V. Pellegrini, R. La Grotta, R. Furlan, G. Matarese, F. Prattichizzo, P. de Candia, Extracellular vesicles as human therapeutics: A scoping review of the literature. *J. Extracell. Vesicles* **13**, e12433 (2024).
42. X. Yu, C. Huang, B. Song, Y. Xiao, M. Fang, J. Feng, P. Wang, $CD4^+CD25^+$ regulatory T cells-derived exosomes prolonged kidney allograft survival in a rat model. *Cell. Immunol.* **285**, 62–68 (2013).
43. C. Théry, K. W. Witwer, E. Aikawa, M. J. Alcaraz, J. D. Anderson, R. Andriantsitohaina, A. Antoniou, T. Arab, F. Archer, G. K. Atkin-Smith, D. C. Ayre, J. M. Bach, D. Bachurski, H. Baharvand, L. Balaj, S. Baldacchino, N. N. Bauer, A. A. Baxter, M. Bebawy, C. Beckham, A. B. Zavec, A. Benmoussa, A. C. Berardi, P. Bergese, E. Bielska, C. Blenkiron, S. Bobis-Wozowicz, E. Boilard, W. Boireau, A. Bongiovanni, F. E. Borràs, S. Bosch, C. M. Boulanger, X. Breakefield, A. M. Breglio, M. Brennan, D. R. Brigstock, A. Brisson, M. L. Broekman, J. F. Bromberg, P. Bryl-Górecka, S. Buch, A. H. Buck, D. Burger, S. Busatto, D. Buschmann, B. Bussolati, E. I. Buzás, J. B. Byrd, G. Camussi, D. R. Carter, S. Caruso, L. W. Chamley, Y. T. Chang, C. Chen, S. Chen, L. Cheng, A. R. Chin, A. Clayton, S. P. Clerici, A. Cocks, E. Cocucci, R. J. Coffey, A. Cordeiro-da-Silva, Y. Couch, F. A. Coumans, B. Coyle, R. Crescitelli, M. F. Criado, C. D'Souza-Schorey, S. Das, A. D. Chaudhuri, P. de Candia, E. F. De Santana, O. De Wever, H. A. Del Portillo, T. Demaret, S. Deville, A. Devitt, B. Dhondt, D. Di Vizio, L. C. Dieterich, V. Dolo, A. P. D. Rubio, M. Dominici, M. R. Dourado, T. A. Driedonks, F. V. Duarte, H. M. Duncan, R. M. Eichenberger, K. Ekström, S. El Andaloussi, C. Elie-Caille, U. Erdbrügger, J. M. Falcón-Pérez, F. Fatima, J. E. Fish, M. Flores-Bellver, A. Försönits, A. Frelet-Barrand, F. Fricke, G. Fuhrmann, S. Gabrielsson, A. Gámez-Valero, C. Gardiner, K. Gärtner, R. Gaudin, Y. S. Gho, B. Giebel, C. Gilbert, M. Gimona, I. Giusti, D. C. Goberdhan, A. Görgens, S. M. Gorski, D. W. Greening, J. C. Gross, A. Gualerzi, G. N. Gupta, D. Gustafson, A. Handberg, R. A. Haraszti, P. Harrison, H. Hegyesi, A. Hendrix, A. F. Hill, F. H. Hochberg, K. F. Hoffmann, B. Holder, H. Holthofer, B. Hosseinkhani, G. Hu, Y. Huang, V. Huber, S. Hunt, A. G. Ibrahim, T. Ikezu, J. M. Inal, M. Isin, A. Ivanova, H. K. Jackson, S. Jacobsen, S. M. Jay, M. Jayachandran, G. Jenster, L. Jiang, S. M. Johnson, J. C. Jones, A. Jong, T. Jovanovic-Talisman, S. Jung, R. Kalluri, S. I. Kano, S. Kaur, Y. Kawamura, E. T. Keller, D. Khamari, E. Khomyakova, A. Khvorova, P. Kierulf, K. P. Kim, T. Kislinger, M. Klingeborn, D. J. Klinke II, M. Kornek, M. M. Kosanović, Á. F. Kovács, E.-M. Krämer-Albers, S. Krasemann, M. Krause, I. V. Kurochkin, G. D. Kusuma, S. Kuypers, S. Laitinen, S. M. Langevin, L. R. Languino, J. Lannigan, C. Lässer, L. C. Laurent, G. Lavieu, E. Lázaro-Ibáñez, S. Le Lay, M. S. Lee, Y. X. F. Lee, D. S. Lemos, M. Lenassi, A. Leszczynska, I. T. Li, K. Liao, S. F. Libregts, E. Ligeti, R. Lim, S. K. Lim, A. Linē, K. Linnemannstöns, A. Llorente, C. A. Lombard, M. J. Lorenowicz, Á. M. Lörincz, J. Lötvall, J. Lovett, M. C. Lowry, X. Loyer, Q. Lu, B. Lukomska, T. R. Lunavat, S. L. Maas, H. Malhi, A. Marcilla, J. Mariani, J. Mariscal, E. S. Martens-Uzunova, L. Martin-Jaular, M. C. Martinez, V. R. Martins, M. Mathieu, S. Mathivanan, M. Maugeri, L. K. McGinnis, M. J. McVey, D. G. Meckes Jr., K. L. Meehan, I. Mertens, V. R. Minciacchi, A. Möller, M. M. Jørgensen, A. Morales-Kastresana, J. Morhayim, F. Mullier, M. Muraca, L. Musante, V. Mussack, D. C. Muth, K. H. Myburgh, T. Najrana, M. Nawaz, I. Nazarenko, P. Nejsum, C. Neri, T. Neri, R. Nieuwland, L. Nimrichter, J. P. Nolan, E. N. Nolte-'t Hoen, N. N. Hooten, L. O'Driscoll, T. O'Grady, A. O'Loghlen, T. Ochiya, M. Olivier, A. Ortiz, L. A. Ortiz, X. Osteikoetxea,

O. Østergaard, M. Ostrowski, J. Park, D. M. Pegtel, H. Peinado, F. Perut, M. W. Pfaffl, D. G. Phinney, B. C. Pieters, R. C. Pink, D. S. Pisetsky, E. Pogge von Strandmann, I. Polakovicova, I. K. Poon, B. H. Powell, I. Prada, L. Pulliam, P. Quesenberry, A. Radeghieri, R. L. Raffai, S. Raimondo, J. Rak, M. I. Ramirez, G. Raposo, M. S. Rayyan, N. Regev-Rudzki, F. L. Ricklefs, P. D. Robbins, D. D. Roberts, S. C. Rodrigues, E. Rohde, S. Rome, K. M. Rouschop, A. Rughetti, A. E. Russell, P. Saá, S. Sahoo, E. Salas-Huenuleo, C. Sánchez, J. A. Saugstad, M. J. Saul, R. M. Schiffelers, R. Schneider, T. H. Schøyen, A. Scott, E. Shahaj, S. Sharma, O. Shatnyeva, F. Shekari, G. V. Shelke, A. K. Shetty, K. Shiba, P. R. Siljander, A. M. Silva, A. Skowronek, O. L. Snyder II, R. P. Soares, B. W. Sódar, C. Soekmadji, J. Sotillo, P. D. Stahl, W. Stoorvogel, S. L. Stott, E. F. Strasser, S. Swift, H. Tahara, M. Tewari, K. Timms, S. Tiwari, R. Tixeira, M. Tkach, W. S. Toh, R. Tomasini, A. C. Torrecilhas, J. P. Tosar, V. Toxavidis, L. Urbanelli, P. Vader, B. W. van Balkom, S. G. van der Grein, J. Van Deun, M. J. van Herwijnen, K. Van Keuren-Jensen, G. van Niel, M. E. van Royen, A. J. van Wijnen, M. H. Vasconcelos, I. J. Vechetti Jr., T. D. Veit, L. J. Vella, É. Velot, F. J. Verweij, B. Vestad, J. L. Viñas, T. Visnovitz, K. V. Vukman, J. Wahlgren, D. C. Watson, M. H. Wauben, A. Weaver, J. P. Webber, V. Weber, A. M. Wehman, D. J. Weiss, J. A. Welsh, S. Wendt, A. M. Wheelock, Z. Wiener, L. Witte, J. Wolfram, A. Xagorari, P. Xander, J. Xu, X. Yan, M. Yáñez-Mó, H. Yin, Y. Yuana, V. Zappulli, J. Zarubova, V. Žėkas, J. Y. Zhang, Z. Zhao, L. Zheng, A. R. Zheutlin, A. M. Zickler, P. Zimmermann, A. M. Zivkovic, D. Zocco, E. K. Zuba-Surma, Minimal information for studies of extracellular vesicles 2018 (MISEV2018): A position statement of the International Society for Extracellular Vesicles and update of the MISEV2014 guidelines. *J. Extracell. Vesicles* **7**, 1535750 (2018).

44. N. Komatsu, K. Okamoto, S. Sawa, T. Nakashima, M. Oh-hora, T. Kodama, S. Tanaka, J. A. Bluestone, H. Takayanagi, Pathogenic conversion of Foxp3$^+$ T cells into T_H17 cells in autoimmune arthritis. *Nat. Med.* **20**, 62–68 (2014).
45. M. Noval Rivas, O. T. Burton, P. Wise, L.-M. Charbonnier, P. Georgiev, H. C. Oettgen, R. Rachid, T. A. Chatila, Regulatory T cell reprogramming toward a T_H2-cell-like lineage impairs oral tolerance and promotes food allergy. *Immunity* **42**, 512–523 (2015).
46. N. van Panhuys, F. Klauschen, R. N. Germain, T-cell-receptor-dependent signal intensity dominantly controls CD4$^+$ T cell polarization in vivo. *Immunity* **41**, 63–74 (2014).
47. V. De Rosa, M. Galgani, A. Porcellini, A. Colamatteo, M. Santopaolo, C. Zuchegna, A. Romano, S. De Simone, C. Procaccini, C. La Rocca, P. B. Carrieri, G. T. Maniscalco, M. Salvetti, M. C. Buscarinu, A. Franzese, E. Mozzillo, A. La Cava, G. Matarese, Glycolysis controls the induction of human regulatory T cells by modulating the expression of *FOXP3* exon 2 splicing variants. *Nat. Immunol.* **16**, 1174–1184 (2015).
48. M. Napolitano, M. Comegna, M. Succoio, E. Leggiero, L. Pastore, R. Faraonio, F. Cimino, F. Passaro, Comparative analysis of gene expression data reveals novel targets of senescence-associated microRNAs. *PLOS ONE* **9**, e98669 (2014).
49. C. Palma, C. La Rocca, V. Gigantino, G. Aquino, G. Piccaro, D. Di Silvestre, F. Brambilla, R. Rossi, F. Bonacina, M. T. Lepore, M. Audano, N. Mitro, G. Botti, S. Bruzzaniti, C. Fusco, C. Procaccini, V. De Rosa, M. Galgani, C. Alviggi, A. Puca, F. Grassi, T. Rezzonico-Jost, G. D. Norata, P. Mauri, M. G. Netea, P. de Candia, G. Matarese, Caloric restriction promotes immunometabolic reprogramming leading to protection from tuberculosis. *Cell Metab.* **33**, 300–318.e12 (2021).
50. D. Szklarczyk, A. L. Gable, D. Lyon, A. Junge, S. Wyder, J. Huerta-Cepas, M. Simonovic, N. T. Doncheva, J. H. Morris, P. Bork, L. J. Jensen, Christian v. Mering, STRING v11: Protein–protein association networks with increased coverage, supporting functional discovery in genome-wide experimental datasets. *Nucleic Acids Res.* **47**, D607–D613 (2018).
51. R. Saito, M. E. Smoot, K. Ono, J. Ruscheinski, P. L. Wang, S. Lotia, A. R. Pico, G. D. Bader, T. Ideker, A travel guide to Cytoscape plugins. *Nat. Methods* **9**, 1069–1076 (2012).
52. S. Maere, K. Heymans, M. Kuiper, BiNGO: A Cytoscape plugin to assess overrepresentation of gene ontology categories in biological networks. *Bioinformatics* **21**, 3448–3449 (2005).
53. D. W. Huang, B. T. Sherman, R. A. Lempicki, Systematic and integrative analysis of large gene lists using DAVID bioinformatics resources. *Nat. Protoc.* **4**, 44–57 (2009).
54. H. Y. Huang, Y. C. Lin, J. Li, K. Y. Huang, S. Shrestha, H. C. Hong, Y. Tang, Y. G. Chen, C. N. Jin, Y. Yu, J. T. Xu, Y. M. Li, X. X. Cai, Z. Y. Zhou, X. H. Chen, Y. Y. Pei, L. Hu, J. J. Su, S. D. Cui, F. Wang, Y. Y. Xie, S. Y. Ding, M. F. Luo, C. H. Chou, N. W. Chang, K. W. Chen, Y. H. Cheng, X. H. Wan, W. L. Hsu, T. Y. Lee, F. X. Wei, H. D. Huang, miRTarBase 2020: Updates to the experimentally validated microRNA-target interaction database. *Nucleic Acids Res.* **48**, D148–D154 (2020).
55. A. Subramanian, P. Tamayo, V. K. Mootha, S. Mukherjee, B. L. Ebert, M. A. Gillette, A. Paulovich, S. L. Pomeroy, T. R. Golub, E. S. Lander, J. P. Mesirov, Gene set enrichment analysis: A knowledge-based approach for interpreting genome-wide expression profiles. *Proc. Natl. Acad. Sci. U.S.A.* **102**, 15545–15550 (2005).
56. P. Palumbo, F. Lombardi, F. R. Augello, I. Giusti, V. Dolo, P. Leocata, M. G. Cifone, B. Cinque, Biological effects of selective COX-2 inhibitor NS398 on human glioblastoma cell lines. *Cancer Cell Int.* **20**, 167 (2020).
57. D. Di Silvestre, F. Brambilla, P. L. Mauri, Multidimensional protein identification technology for direct-tissue proteomics of heart. *Methods Mol. Biol.* **1005**, 25–38 (2013).
58. A. Dobin, C. A. Davis, F. Schlesinger, J. Drenkow, C. Zaleski, S. Jha, P. Batut, M. Chaisson, T. R. Gingeras, STAR: Ultrafast universal RNA-seq aligner. *Bioinformatics* **29**, 15–21 (2013).
59. Y. Liao, G. K. Smyth, W. Shi, featureCounts: An efficient general purpose program for assigning sequence reads to genomic features. *Bioinformatics* **30**, 923–930 (2014).
60. G. Yu, L. G. Wang, Y. Han, Q. Y. He, clusterProfiler: An R package for comparing biological themes among gene clusters. *OMICS* **16**, 284–287 (2012).
61. P. Campomenosi, E. Gini, D. M. Noonan, A. Poli, P. D'Antona, N. Rotolo, L. Dominioni, A. Imperatori, A comparison between quantitative PCR and droplet digital PCR technologies for circulating microRNA quantification in human lung cancer. *BMC Biotechnol.* **16**, 60 (2016).

Acknowledgments: Schematic figures were created with images adapted from Smart Servier Medical Art (https://smart.servier.com/) and BioRender.com. We thank E. Bulgheroni for technical help, D. Di Vizio for manuscript revision, and T. Russo for fruitful discussions and continuous support. **Funding:** This work was supported by Federazione Italiana Sclerosi Multipla, grant 2016/R/10 (to P.d.C.); National Multiple Sclerosis Society, grant PP-1606-24687 (to P.d.C.); Federazione Italiana Sclerosi Multipla, grant 2018/R/4 (to P.d.C.); Juvenile Diabetes Research Foundation, grant 1-SRA-2018-477-S-B (to P.d.C.); National Recovery and Resilience Plan (NRRP), Mission 4, Component 2 (M4C2), Investment 1.1, call for tender no. 104 published on 2 February 2022 by the Italian Ministry of University and Research (MUR), funded by the European Union–NextGenerationEU–project title: PLasmatic extracellular vesicles AT the INtersection of immune and metabolic dysregulation in Obesity and type 2 diabetes (PLATINO–Protocol 20228BRER5_002, CUP E53D2301227 0001–Grant Assignment Decree No. 1065 adopted on 18 July 2023 (to P.d.C.); NRRP, M4C2, Investment 1.1, call for tender no. 1409 published on 14 September 2022 by the Italian Ministry of University and Research (MUR), funded by the European Union–NextGenerationEU–project title: An integrated plasma circulating PROtein-MIRNA SIgnature in type 1 diabetes: Markers and players of disease progression (PROMISI)–Protocol P2022H8MZ4, CUP E53D2301541 0001–Grant Assignment Decree No. 1364 adopted on 1 September 2023 (to P.d.C.); Federazione Italiana Sclerosi Multipla, grant 2022-PR-Single/013 (to C.P.); Italian Ministry of Health, Next Generation EU, M6/C2_CALL 2022 cod. PNRR-MAD-2022-12376126, project title: Immune-nervous system interplay in multiple sclerosis: Understanding the role of catecholamines in the control of neuronal and immune dysfunctions (to C.P.); National Recovery and Resilience Plan (NRRP), Mission 4, Component 2 (M4C2), Investment 1.1, call for tender no. 1409 published on 14 September 2022 by the Italian Ministry of University and Research (MUR), funded by the European Union–NextGenerationEU–project title: Defining the role of the mTORC1-TFEB axis in the control of immune tolerance in multiple sclerosis (P2022T4PKT)-CUP B53D23024820001–Grant Assignment Decree No. 1365 published on 1 September 2023 (to C.P.); National Recovery and Resilience Plan (NRRP), Mission 4, Component 2 (M4C2), Investment 1.1, call for tender no. 104 published on 2 February 2022 by the Italian Ministry of University and Research (MUR), funded by the European Union–NextGenerationEU–project title: Role of overweight and EBV infection in the pathogenesis of multiple sclerosis: Metabolic overwork as key mechanism leading to loss of immune-tolerance (grant no. 2022LNHZAP)–CUP E53D23013240006–Grant Assignment Decree No. 0001111 adopted on 20 July 2023 (to G. Matarese); Italian Ministry of Health, Next Generation EU, M6/C2_CALL 2022 cod. PNRR-MAD-2022-12375634, project title: Innate immune CElls in MUltiple SCLErosis – ICEMUSCLE (to R.F.); Italian National Recovery and Resilience Plan (PNRR), project code: PNRR-MCNT2-2023-12378040, M6/C2_CALL 2023, funded by Ministero della Salute, title: Measuring immunological self-tolerance reservoir to validate innovative therapies in patients with relapsing-remitting multiple sclerosis (to G. Matarese); MUR/PNRR Extended Partnership (MNESYS no. PE00000006) (to G. Matarese, A.U., and D. Centonze); Ministry of Health, Bando Ricerca Finalizzata 2021 (grant no. GR-2021-12373337) (to F.C.); National Recovery and Resilience Plan (NRRP), Mission 4, Component 2 (M4C2), Investment 1.1, call for tender no. 104 published on 2 February 2022 by the Italian Ministry of University and Research (MUR), funded by the European Union–NextGenerationEU–project title: Role of metabolic pressure and viral infections in the loss of immune tolerance and tissue damage in celiac disease (grant no. 2022YMJXYT)–CUP B53D23003710006–Grant Assignment Decree No. 972 adopted on 30 June 23 (to F.C.); and National Recovery and Resilience Plan (NRRP), M4C2, Investment 1.1, call for tender no. 104 published on 2 February 2022 by the Italian Ministry of University and Research (MUR), funded by the European Union–NextGenerationEU–project title: Regulatory T cell-mediated immunological nursing for direct cardiac reprogramming (IMMUNOCARD) (grant no. 20225KH7BZ)–CUP B53D23012500006–Grant Assignment Decree No. 971 adopted on 30 June 23 (to C.L.R.). **Author contributions:** P.d.C and C.P. served as co–senior authors. P.d.C. designed the initial study, and P.d.C., C.P., G.D.R., and G. Matarese planned the experiments throughout the study progress. P.d.C., C.P., G.D.R., C.R., D.D.S., S.G., C.F., A.C., C.L.R., F. Passaro, F. Brambilla, M.H., I.G., P.D.A., V.M., A.R., and A.F. participated in the development of adequate methodologies for addressing the scientific questions. P.d.C., C.P., G.D.R., C.R., D.D.S., S.G., I.S., G. Mele, F.C., A.F., I.M., A.M., C.F., A.C., C.L.R., F. Passaro, V.B., V.D., P.C., P.B., and R.F. performed the experiments, and P.d.C., C.P., G.D.R., C.R., D.D.S., D. Carpi, and E.T. did data analysis. F. Buttari, D. Centonze, G.A., S.B., F. Beretta, E.D.S., G.C., E.D., G.L., E.S., R.L., V.B.M., M.M., and B.Z. were in charge of human sample and data acquisition. P.d.C., C.P., G. Matarese, and R.F. acquired the funding. P.d.C., C.P., and G. Matarese administered and supervised the project. P.d.C., C.P., and G.D.R. collaborated in the original draft writing. P.d.C., C.P., G.D.R., C.R., D.D.S., F. Prattichizzo, P.M., V.B., V.D., P.C., P.B., A.U., M.S., D. Centonze, R.F., and G. Matarese concurred to

reviewing and editing of the manuscript and its scientific content. **Competing interests:** The authors declare that they have no competing interests. **Data and materials availability:** All data associated with this study are present in the paper or the Supplementary Materials. Isolation and characterization protocols for T cell–derived EVs can be found at EV-track (EV210300). Proteomics data for EV-treated $CD4^+$ T cells can be found at MassIVE (MSV000088391). Microarray data for human T_{conv} cell stimulation, RT-qPCR data of EV-associated miRNAs from human T_{conv} cells, RT-qPCR data of EV-associated miRNAs from human T_{reg} cells, and RNA-seq data of EV-treated $CD4^+$ T cells can be found at the Gene Expression Omnibus (accession numbers: GSE154401, GSE183713, GSE209714, and GSE208570, respectively).

Submitted 4 October 2023
Resubmitted 21 October 2024
Accepted 4 April 2025
Published 28 May 2025
10.1126/scitranslmed.adl1698